Infrared Spectra of the CH_3-MX, $CH_2=MHX$, and $CH\equiv MH_2X^-$ Complexes Formed by Reaction of Methyl Halides with Laser-ablated Group 5 Metal Atoms

Han-Gook Cho and Lester Andrews*

Department of Chemistry, University of Incheon, 177 Dohwa-dong, Nam-ku, Incheon, 402-749, South Korea, and Department of Chemistry, University of Virginia, P.O. Box 400319, Charlottesville, Virginia 22904-4319

Received: May 15, 2006; In Final Form: June 16, 2006

Reactions of group 5 metal atoms and methyl halides give carbon−metal single, double, and triple bonded complexes that are identified from matrix IR spectra and vibrational frequencies computed by DFT. Two different pairs of complexes are prepared in reactions of methyl fluoride with laser-ablated vanadium and tantalum atoms. The two vanadium complexes (CH_3-VF and $CH_2=VHF$) are persistently photoreversible and show a kinetic isotope effect on the yield of $CD_2=VDF$. Identification of $CH_2=TaHF$ and $CH\equiv TaH_2F^-$, along with the similar anionic Nb complex, suggests that the anionic methylidyne complex is a general property of the heavy group 5 metals. Reactions of Nb and Ta with CH_3Cl and CH_3Br have also been carried out to understand the ligand effects on the calculated structures and the vibrational characteristics. The methylidene complexes become more distorted with increasing halogen size, while the calculated C=M bond lengths and stretching frequencies decrease and increase, respectively. The anionic methylidyne complexes are less favored with increasing halogen size. Infrared spectra show a dramatic increase of the Ta methylidenes upon annealing, suggesting that the formation of CH_3-TaX and its conversion to $CH_2=TaHX$ require essentially no activation energy.

Introduction

Recent investigations of group 4, 5, and 6 transition-metal atom reactions with methane and methyl halides in our laboratories have discovered a new class of simple methylidene complexes[1−16] that are relevant model systems for much larger high oxidation-state transition-metal complexes, which often have important catalytic properties for methathesis reactions of alkenes, alkynes, and cyclic compounds.[17] The small complexes often possess agostically distorted structures and show interesting matrix effects. Many of the systems also show fascinating photochemistry, including persistent photoreversibilities and dramatic product increases. Close examination of ligand effects on the agostic interaction[18] have also been discussed.[8,9]

Previous studies show progressive variations in the reactivity of the early transition metals moving horizontally and vertically in the periodic table. Group 4 metals produce single- and double-bonded (methyl and methylidene) complexes in reaction with methane and methyl halides, and more stable higher-order complexes ($(CH_3)_2MX_2$, X = H, F, Cl, Br) are also formed particularly at high concentration and upon annealing.[1−4,6,7] Group 6 metals yield single-, double-, and triple-bonded (methyl, methylidene, and methylidyne) complexes; however, the higher-order complex, $(CH_3)_2MX_2$, is not identified.[10−13] Group 5 metals, on the other hand, form single, double, and anionic triple bonded ($CH\equiv MH_2X^-$) complexes along with $(CH_3)_2MX_2$.[14,15] The primary reaction products of early first-row transition metals are insertion complexes, and the higher oxidation-state complexes are formed upon irradiation via α-hydrogen migration.[1−3] The higher oxidation-state complexes are favored in the reaction of second- and third-row transition metals.[4−9] In contrast, late first-row transition metals and Rh give only insertion complexes.[19−22]

Reactions of group 5 transition metals with methyl halides are relatively less studied in comparison with group 4 and 6 metals. The CH_3-NbF, $CH_2=NbHF$, and $CH\equiv NbH_2F^-$ complexes have been prepared recently in the reaction of Nb + CH_3F,[14] and similar products with group 5 metals and CH_4 have been identified.[15] In this investigation, reactions of laser-ablated group 5 metal atoms with methyl halides diluted in argon were carried out, and the products isolated in an argon matrix were investigated by means of IR spectroscopy. A photoreversible system is found from the products of V + CH_3F, and parallel to the case of Nb, the anionic methylidyne complex is one of the major products in the reaction of Ta with CH_3F. Further examination of reactions of Nb and Ta with CH_3Cl and CH_3Br have also been done to understand the halide ligand effect. Products are identified by the effect of isotopic substitution on the IR spectrum and complementary density functional theory (DFT) frequency calculations.

Experimental and Computational Methods

Laser-ablated group 5 metal atoms (Johnson-Matthey) were reacted with CH_3X isotopomers (CH_3F (Matheson), $^{13}CH_3F$, CH_3Cl, CH_3Br, CD_3Br (Cambridge Isotopic Laboratories, 99%), CD_3F (synthesized from CD_3Br and HgF_2), and CD_3Cl (synthesized from CD_3Br and $HgCl_2$)) in excess argon during condensation at 8 K using a closed-cycle refrigerator (Air Products HC-2). The methods have been described in detail elsewhere.[23,24] The concentrations of gas mixtures are typically 0.2−0.5% in argon. In addition, CCl_4 was added (0.05%) in the gas mixture to capture electrons produced in the laser-ablation process.[24] After reaction, IR spectra were recorded at a resolution of 0.5 cm^{-1} using a Nicolet 550 spectrometer with an MCT-B detector. Samples were later irradiated by a mercury arc lamp (175 W) with a combination of optical filters, were annealed, and more spectra were recorded.

* To whom correspondence should be addressed. E-mail: lsa@virginia.edu.

10.1021/jp0629644 CCC: $33.50
Published on Web 08/01/2006

TABLE 1: Frequencies of Product Absorptions Observed from Reactions of Methyl Fluoride with Group 5 Metals in Excess Argon[a]

	V			Nb[b]			Ta			
group	CH_3F	CD_3F	$^{13}CH_3F$	CH_3F	CD_3F	$^{13}CH_3F$	CH_3F	CD_3F	$^{13}CH_3F$	description
i	1117.8	880.7	1108.5							CH_3 deform
	653.1, 656.9	651.4	652.8	629.7, 627.4	629.2, 627.8	629.3, 627.2				M−F str.
	521.7	461.2	512.6							C−M str.
h	619.0	617.3	618.9							V−F str.
m	1685.8, 1678.1	1217.9	1686.0, 1678.0	**1698.7**, 1681.7	**1220.9**, 1208.3	**1698.6**, 1681.8	1765.0, 1759.3	1263.8, 1260.3	1765.1, 1760.3	M−H str.
	779.8	710.8	769.4	**777.7**, 772.9	695.8, **683.8**	758.6	809.8	686.6	789.1	C═M str.
	713.5		707.2	694.3	634.3, **632.3**	693.9, **691.4**	702.9, 700.1	660.6, 658.9	701.0, 698.4	M−F str.
	641.9	**510.5**, 502.9	637.9	**651.0**, 646.1	**537.3**, 535.1	**645.8**, 640.8	672.9	526.7	665.6	CH_2 wag
	625.5		624.6	612.4		611.3	621.0		620.3	CMH bend
a				1560.4	1120.4	1560.3	1643.8		1643.6	MH_2 str.
				1526.7	1103.0	1526.7	1608.0	1156.1	1608.0	MH_2 str.
				899.4		872.3	913.3		883.4	C≡M str.
							637.5		636.4	MH_2 bend
				617.8	573.0	617.1	612.0	579.8	611.4	M−F str.
				547.9		545.7	578.8		574.6	MCH bend
				512.0		512.0				MH_2 deform.

[a] All frequencies are in cm^{-1}. Stronger absorptions are bold. Description gives the major coordinate. [b] Reference 14.

TABLE 2: Calculated Fundamental Frequencies of CH_3−MF Isotopomers in the Ground $^4A''$ Electronic State[a]

approximate	V				Nb				Ta			
description	CH_3−VF	int.	CD_3−VF	$^{13}CH_3$−VF	CH_3−NbF	int.[b]	CD_3-NbF	$^{13}CH_3$−NbF	CH_3−TaF	int.[b]	CD_3−TaF	$^{13}CH_3$−TaF
A′ CH_3 str.	3097.8	4	2287.5	3087.6	3114.7	1	2298.6	3104.7	3105.2	1	2291.2	3095.2
A′ CH_3 str.	2970.8	7	2131.8	2967.4	2943.8	3	2114.9	2940.0	2950.5	3	2120.5	2946.7
A′ CH_3 scis.	1417.0	2	1028.2	1413.9	1405.6	4	1020.5	1402.4	1408.4	7	1021.5	1405.4
A′ CH_3 deform	1153.2	4	904.8	1144.0	1160.3	14	914.5	1150.5	1175.8	21	925.2	1166.0
A′ M−F str.	668.8	176	666.9	668.5	639.5	149	639.0	639.4	632.6	109	629.9	632.0
A′ C−M str.	546.4	46	475.7	537.7	562.7	30	484.5	552.1	549.5	32	473.8	538.9
A′ CH_3 rock	422.9	25	340.7	416.8	381.6	28	311.0	375.8	397.7	25	317.9	391.8
A′ CMF bend	135.9		127.5	135.1	145.3	2	135.3	144.7	127.0	0	118.6	126.0
A″ CH_3 str.	3028.4	9	2236.3	3018.1	2996.3	4	2211.5	2986.2	3002.3	4	2215.7	2992.2
A″ CH_3 scis.	1428.9	1	1036.4	1425.7	1415.5	4	1027.4	1412.3	1413.8	6	1025.6	1410.6
A″ CH_2 twist	411.5	22	307.8	409.5	365.7	5	272.0	364.1	390.0	3	290.1	388.2
A″ HCMF distort	77.7	2	56.1	77.6	88.8	0	64.9	88.7	74.6	0	54.1	74.3

[a] Calculated using B3LYP/6-311++G(3df, 3pd) and the SDD core potential and basis set for Nb and Ta. Frequencies and intensities are in cm^{-1} and km/mol. Infrared intensities are calculated values for the product of CH_3F.

TABLE 3: Calculated Fundamental Frequencies of Group 5 Metal Methylidene (CH_2═MHF) Isotopomers in the Ground ^1A Electronic State[a]

approximate	V				Nb				Ta			
description	CH_2═VHF	int.	CD_2═VDF	$^{13}CH_2$−VHF	CH_2═NbHF	int.	CD_2═NbDF	$^{13}CH_2$═NbHF	CH_2═TaHF	int.	CD_2═TaDF	$^{13}CH_2$═TaHF
C−H str.	3211.8	1	2377.3	3200.8	3210.4	3	2377.1	3199.4	3223.2	3	2386.5	3212.1
C−H str.	2845.9	2	2069.0	2839.5	2840.5	4	2067.6	2833.9	2838.5	6	2067.2	2831.8
M−H str.	1751.3	264	1252.9	1751.3	1755.0	284	1248.9	1755.0	1803.6	243	1279.8	1803.6
CH_2 scis.	1322.1	25	1029.1	1313.0	1334.6	21	1047.9	1325.4	1334.6	20	1045.5	1325.7
C═M str.	774.9	177	719.0	772.3	810.4	72	710.9	791.8	815.8	51	714.7	794.3
M−F str.	709.5	13	626.5	696.3	727.1	89	667.4	723.7	706.9	88	658.9	705.0
CH_2 wag	661.4	117	521.3	655.4	710.4	93	557.2	704.2	712.1	77	557.8	705.9
CMH bend	634.8	43	508.5	633.6	633.5	55	516.1	632.8	623.9	41	496.3	623.1
CH_2 twist	442.0	14	328.7	441.2	470.9	4	334.8	470.9	447.1	5	318.3	447.0
CH_2 rock	373.1	11	287.7	369.6	394.3	4	314.1	390.8	384.9	4	307.8	381.1
MH o−o-p bend	200.8	54	164.6	200.2	42.9	51	33.0	42.7	108.2	23	81.4	108.1
CMF bend	117.5	67	98.5	117.0	186.9	2	164.4	185.7	174.1	2	153.0	172.8

[a] Frequencies and intensities computed at the level of B3LYP/6-311++G(3df, 3pd), and SDD core potential and basis set are used for Nb and Ta. Frequencies and intensities are in cm^{-1} and km/mol. Intensities are calculated values for the product of CH_3F. CH_2═VHF has a near planar structure, whereas CH_2═NbHF and CH_2═TaHF have planar structures.

Complementary DFT calculations were carried out using the Gaussian 03 package,[25] B3LYP density functional,[26] 6-311++G-(3df,3pd) basis sets[27] for C, H, F, V, and SDD pseudopotential and basis set[28] for Nb and Ta to provide a consistent set of vibrational frequencies for the reaction products. Geometries were fully relaxed during optimization, and the optimized geometry was confirmed by vibrational analysis. Moeller-Plesset second-order perturbation theory (MP2) calculations were also done for the reaction products to confirm the DFT results. All of the vibrational frequencies were calculated analytically. In the calculation of binding energy of a metal complex, the zero-point energy is included.

Calculations on transition-metal compounds are difficult, and DFT is approximate for both relative stabilities and vibrational frequencies. This can be seen from Tables 1−3, which show that the V−F stretching frequency calculated for CH_3−VF is about 16 cm^{-1} lower than the experimental value while that for CH_2═VHF is about 4 cm^{-1} higher, indicating that the B3LYP functional does not describe both structures consistently, but it does predict frequencies that are close to the observed

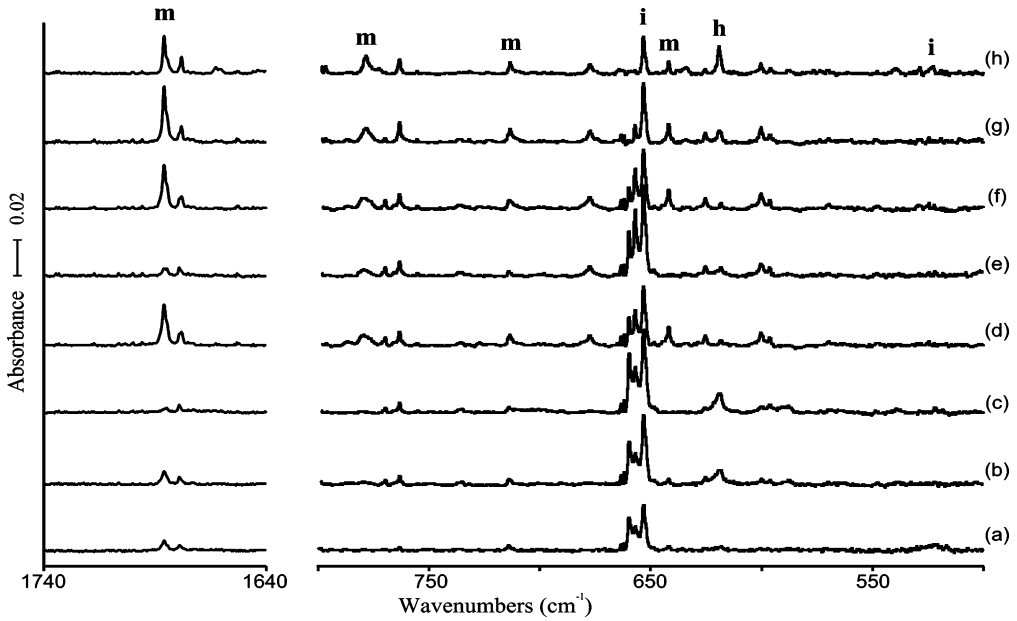

Figure 1. IR spectra in the regions of 1740−1640 and 800−620 cm^{-1} for laser-ablated V atoms co-deposited with CH_3F in excess argon at 8 K and their variation. (a) V + 0.2% CH_3F in Ar co-deposited for 1 h. (b) V + 0.5% CH_3F in Ar co-deposited for 1 h. (c) After broad-band photolysis with a filter (λ > 420 nm) for 20 min. (d) After broad-band photolysis with a filter (240 < λ < 380 nm) for 20 min. (e) After broad-band photolysis with a filter (λ > 420 nm) for 20 min. (f) After broad-band photolysis with a filter (240 < λ < 380 nm) for 20 min. (g) After annealing to 28 K. (h) After annealing to 44 K. **i**, **h**, and **m** denote the product absorption group.

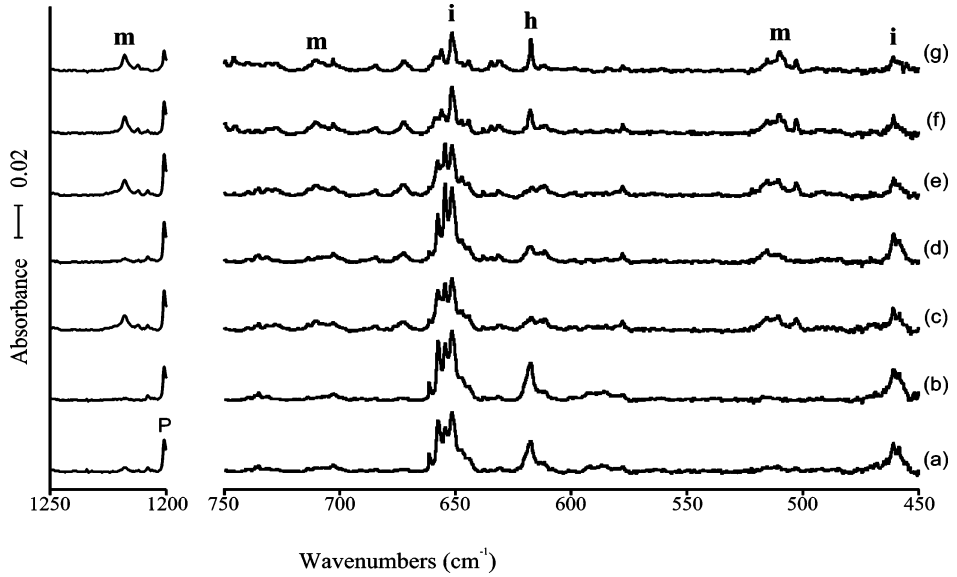

Figure 2. IR spectra in the regions of 1250−1200 and 750−450 cm^{-1} for laser-ablated V atoms co-deposited with CD_3F in excess argon at 8 K and their variation. (a) V + 0.5% CH_3F in Ar co-deposited for 1 h. (b) After broad-band photolysis with a filter (λ > 420 nm) for 20 min. (c) After broad-band photolysis with a filter (240 < λ < 380 nm) for 20 min. (d) After broad-band photolysis with a filter (λ > 420 nm) for 20 min. (e) After broad-band photolysis with a filter (240 < λ < 380 nm) for 20 min. (f) After annealing to 30 K. (g) After annealing to 38 K. **i**, **h**, and **m** denote the product absorption group, and P indicates precursor absorption.

values. The harmonic approximation was used for the frequency calculations, the effect of anharmonicity was not included, and no scale factors were used for calculated frequencies reported here. Finally, calculations were performed for the gaseous species, and the frequencies are measured in an argon matrix, which typically results in a small 1−2% red shift in the vibrational frequencies.

Results and Assignments

Reactions of V, Nb, and Ta with methyl halide isotopomers were done in condensing argon, and the observed product vibrational characteristics and their variations upon photolysis and annealing are compared with the calculated results.

V + CH_3F. Two sets of product absorptions are observed on the basis of the behaviors upon photolysis and annealing as listed in Table 1. The IR spectra in the regions of 1740−1640 and 800−620 cm^{-1} from the reaction of laser-ablated V atoms with CH_3F are shown in Figure 1, which includes spectra with 0.2% CH_3F (a) and 0.5% CH_3F and their variation upon photolysis and annealing (b−h). The absorptions marked "**m**" and "**i**" are almost completely photoreversible; an increase of one set of absorptions upon photolysis is accompanied with a decrease of the other set of absorptions. The absorptions marked "**i**" increase upon visible (λ > 420 nm) irradiation while the absorptions marked "**m**" almost disappear. UV (240 < λ < 380 nm) irradiation reverses the effect, and the photoreversibility is

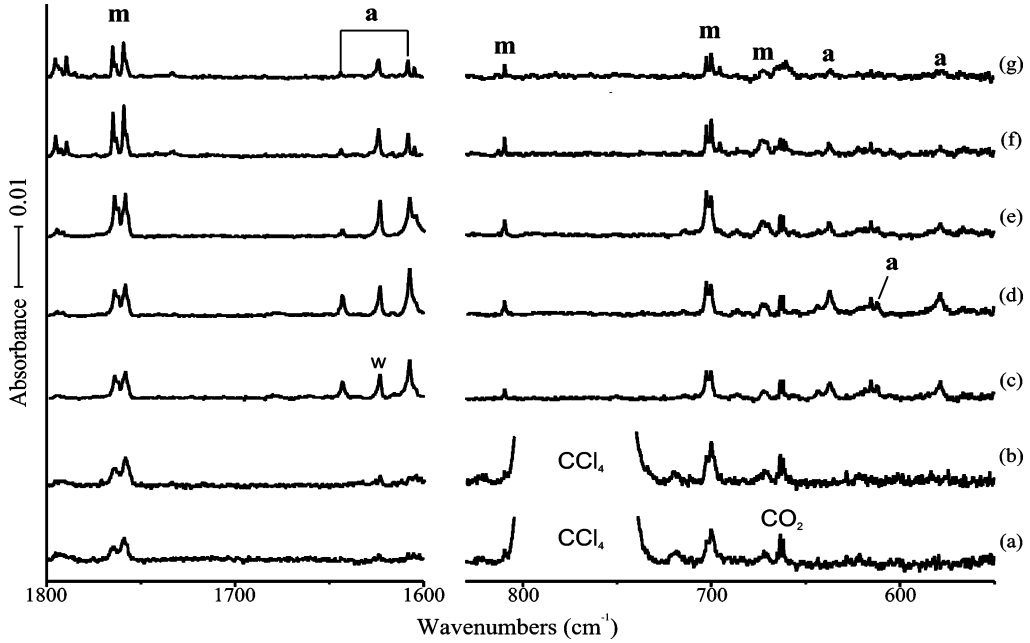

Figure 3. IR spectra in the regions of 1800−1600 and 830−550 cm^{-1} for laser-ablated Ta atoms co-deposited with CH_3F in excess argon at 8 K and their variation. (a) Ta + [0.5% CH_3F + 0.05% CCl_4] in Ar co-deposited for 1 h. (b) After broad-band photolysis with a filter (λ > 420 nm) for 20 min. (c) Ta + 0.5% CH_3F in Ar co-deposited for 1 h. (d) After broad-band photolysis with a filter (λ > 380 nm) for 20 min. (e) After broad-band photolysis with a filter (240 < λ < 380 nm) for 20 min. (f) After annealing to 20 K. (g) After annealing to 28 K. **m** and **a** denote the product absorption group. w, CCl_4, and CO_2 indicate the water, CCl_4, and CO_2 absorptions, respectively.

quite persistent as shown in Figure 1. In the following process of annealing, the absorptions sharpen and decrease.

In the original spectra after deposition (a and b), the **m** absorptions are weak but they increase more than 10-fold later upon UV irradiation (d) as shown in Figures 1 and 2. Clearly, the primary product of the reaction between laser-ablated vanadium atoms and CH_3F is responsible for the **i** absorptions, and the primary product is converted to another product upon UV irradiation, leading to the dramatic increase of the **m** absorptions. We will show below that the **i** and **m** absorptions arise from CH_3-VF and $CH_2{=}VHF$, respectively.

Figure 2 shows the IR spectra in the regions of 1250−1200 and 750−450 cm^{-1} for laser-ablated V atoms co-deposited with Ar/CD_3F at 8 K (a) and their variation upon photolysis and annealing (b−g). The same photoreversibility is observed; the **i** absorptions increase and decrease upon visible and UV irradiation, respectively, while the **m** absorptions decrease and increase instead. In the spectra of deuterated precursors, the absorptions of the methylidene complexes (marked "**m**") are relatively weaker while methylmetal complexes (marked "**i**") are stronger compared with the hydrogen counterparts. If the photochemical absorption coefficients are isotopically invariant, then this difference in relative **i** and **m** absorption intensities for H and D isotopes is probably due to slower α-deuterium migration. In Figures 1 and 2, absorptions marked with "**h**" are also observed, and the **h** band is much weaker at lower concentration as shown in Figure 1a.

The observed product absorptions are assigned on the basis of calculation results, variation of vibrational characteristics upon isotope substitution, and previous results of similar small transition-metal complexes. Calculated vibrational characteristics for the methyl and methylidene complexes (CH_3-VF and $CH_2{=}VHF$) are listed in Tables 2 and 3. A group of **i** absorptions, which are probably a result of site splittings, are observed at about 656 cm^{-1} (the strongest one at 653.1 cm^{-1}) in Figure 1. A similar group of **i** absorptions with almost identical intensity distribution are observed at about 654 cm^{-1} (the strongest one at 651.4 cm^{-1}) in Figure 2. They show ^{13}C and D isotopic shifts of 0.3 and 1.7 cm^{-1} ($^{12}C/^{13}C$ and H/D ratios of 1.001 and 1.003). On the basis of the strong absorption intensities and the small isotopic shifts, the product bands are attributed to the V−F stretching mode.

A weaker **i** absorption is observed at 521.7 cm^{-1} in Figure 1, which shows ^{13}C and D isotopic shifts of −9.1 and −60.5 cm^{-1} ($^{12}C/^{13}C$ and H/D ratios of 1.018 and 1.131). The relatively large ^{13}C shifts indicate that the absorption originates from a vibrational mode involving a large displacement of the carbon atom. The band is assigned to the C−M stretching mode, which is expected to be the second strongest band of CH_3-VF. Another weak **i** absorption is observed at 1117.8 cm^{-1} (not shown) which exhibits ^{13}C and D isotopic shifts of −9.3 and −237.1 cm^{-1} ($^{12}C/^{13}C$ and H/D isotopic ratios of 1.008 and 1.269). The frequency and large deuterium shift indicate that the band arises from the CH_3 deformation mode. The vibrational characteristics of the observed **i** absorptions suggest that they originate from a product with C−F, C−M, and CH_3 moieties. The most plausible reaction product that satisfies the observed vibrational characteristics of the **i** absorptions is CH_3-VF.

The behavior of the absorptions marked "**h**" upon photolysis in Figures 1 and 2 is in part similar to that of the **i** absorptions. They are evident after deposition and increase upon visible irradiation but almost disappear upon UV irradiation. However, they slightly increase in the following visible irradiation and behave photoreversibly. More importantly, they increase dramatically in the process of annealing, and their intensities are much stronger at higher reagent concentration (Figure 1a). The $^{12}C/^{13}C$ and H/D isotopic shifts are similar to those of the V−F stretching absorption of CH_3-VF (0.1 and 1.7 cm^{-1}). The **h** absorptions most probably arise from a weakly bound high-order complex of CH_3-VF with CH_3F, $CH_3-VF\cdots CH_3F$. The excess UV energy probably leads to dissociation of the weakly bound complex, but it is produced again upon annealing.

The absorptions marked "**m**" undergo dramatic variations in intensity upon irradiations as shown in Figures 1 and 2. They

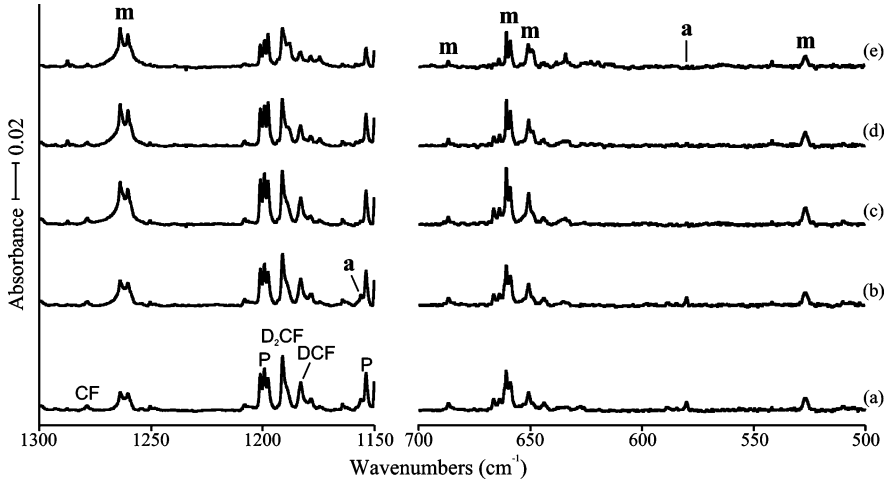

Figure 4. IR spectra in the regions of 1300−1150 and 700−500 cm^{-1} for laser-ablated Ta atoms co-deposited with CD_3F in excess argon at 8 K and their variation. (a) Ta + 0.5% CD_3F in Ar co-deposited for 1 h. (b) After broad-band photolysis with a filter ($\lambda > 420$ nm) for 20 min. (c) After broad-band photolysis with a filter ($240 < \lambda < 380$ nm) for 20 min. (d) After annealing to 28 K. (e) After annealing to 42 K. **m** and **a** denote the product absorption group, and P stands for precursor absorption. CF, D_2CF, and DCF indicate absorptions by the radicals, respectively.[25]

TABLE 4: Calculated Fundamental Frequencies of Group 5 Metal $CH\equiv MH_2F^-$ Isotopomers in the Ground $^1A'$ Electronic State[a]

approximate description	V				Nb				Ta			
	$CH\equiv VHF^-$	int.	$CD\equiv VD_2F^-$	$^{13}CH\equiv VH_2F^-$	$CH\equiv NbH_2F^-$	int.	$CD\equiv NbD_2F^-$	$^{13}CH\equiv NbH_2F^-$	$CH\equiv TaH_2F^-$	int.	$CD\equiv TaH_2F^-$	$^{13}CH\equiv TaH_2F^-$
A′ C−H str.	3093.6	17	2294.5	3082.7	3110.6	14	2306.1	3099.7	3137.2	15	2325.4	3126.3
A′ MH_2 str.	1638.7	464	1168.5	1638.6	1621.8	434	1152.7	1621.7	1674.5	395	1187.8	1674.4
A′ C≡M str.	992.4	126	953.0	965.6	951.7	140	911.3	922.7	936.3	129	894.8	905.5
A′ MH_2 bend	680.1	184	479.4	678.2	619.4	62	464.2	618.3	646.0	160	464.2	645.7
A′ M−F str.	617.7	110	634.1	616.7	617.6	289	570.5	616.5	608.5	102	569.3	608.3
A′ MCH bend	549.3	64	410.9	548.2	547.8	100	417.4	545.2	586.4	130	449.0	582.0
A′ MH_2 wag	473.7	50	369.4	470.9	488.6	40	375.4	488.0	506.2	30	391.8	505.9
A′ CMF bend	228.0	3	205.7	225.4	223.4	4	208.0	220.2	216.2	6	203.2	212.9
A″ MH_2 str.	1603.3	672	1155.7	1603.1	1585.3	675	1133.2	1585.2	1637.6	577	1164.9	1637.6
A″ CH o−o-p bend	675.0	0	538.1	668.5	641.6	13	510.5	635.3	644.1	59	508.2	638.3
A″ MH_2 deform	505.1	119	364.5	504.8	519.2	122	369.6	519.2	544.1	74	388.4	543.8
A″ MH_2 rock	307.8	1	234.5	307.6	319.1	15	243.4	318.8	316.4	15	239.6	316.0

[a] B3LYP/6-311++G(3df,3pd) level and for Nb and Ta, SDD core potential and basis set are used. Frequencies and intensities are in cm^{-1} and km/mol. Intensities are calculated values for the product of CH_3F.

sharpen and later decrease in the process of annealing. Among the absorptions marked "**m**" in Figure 1, the absorption at 1698.7 cm^{-1} is the most distinctive. It shows essentially no ^{13}C shift (−0.1 cm^{-1}) and a large deuterium shift of −467.9 cm^{-1} ($^{12}C/^{13}C$ ratio of 1.391), indicating that it is a hydrogen stretching absorption. The hydrogen stretching absorptions of binary vanadium hydrides have been observed in the same frequency region[29,30] but are not found in this study. This clearly shows that H-atom transfer readily occurs from CH_3-VF upon UV irradiation to form the methylidene complex, $CH_2=VHF$. Therefore, the **m** absorptions in Figures 1 and 2 showing the same behavior upon photolysis and annealing most likely originate from $CH_2=VHF$.

The **m** absorption at 779.8 cm^{-1} shows ^{13}C and D isotope shifts of −10.4 and −69.0 cm^{-1} ($^{12}C/^{13}C$ and H/D ratios of 1.014 and 1.097), and on the basis of the frequency and relatively large ^{13}C shift, it is attributed to the C=V stretching mode. The **m** absorption at 713.5 cm^{-1} shows a ^{13}C shift of −6.3 cm^{-1} (the deuterium counterpart is probably overlapped by another absorption in the congested area). The band is assigned to the V−F stretching mode, which is heavily mixed with the CVH in-plane bending mode. Another strong **m** absorption at 641.9 cm^{-1} shows ^{13}C and D shifts of −4.0 and −131.4 cm^{-1} ($^{12}C/^{13}C$ and H/D ratios of 1.006 and 1.257) and is attributed to the CH_2 wagging mode. The absorption at 625.5 cm^{-1} shows a small ^{13}C shift of −0.9 cm^{-1}, but the deuterium counterpart is not observed probably due to its low frequency. The absorption is assigned to the CVH in-plane bending mode.

The vibrational characteristics of the observed **m** absorptions, consistent with those of previously studied group 4, 5, and 6 metal methylidene complexes,[1−16] affirm the formation of the vanadium methylidene complex ($CH_2=VHF$). Therefore, the photoreversibility between **i** and **m** absorptions is caused by interconversion between the methyl and methylidene complexes (CH_3-VF and $CH_2=VHF$) via α-hydrogen migration, and this process shows a clean deuterium kinetic isotope effect on product yields.

Ta + CH_3F. The spectra observed from the Ta + CH_3F reaction products are shown in Figure 3. Two sets of product absorptions are observed on the basis of variations in intensity upon photolysis, annealing, and addition of CCl_4. The absorptions marked "**m**" are evident after deposition (c) and increase about 20% upon visible irradiation (d). Their intensities almost double in total on UV irradiation (e), and they sharpen and later decrease in the process of annealing (f and g). The absorptions marked "**a**" are also obvious after deposition (c). They increase about 30% upon visible irradiation (d) but dramatically decrease upon UV irradiation and become about half as strong in comparison with the original ones (e). They continuously decrease in annealing (f and g). More importantly, the **a** absorptions almost completely disappear with addition of CCl_4 (a) and they are not discernible even after following visible

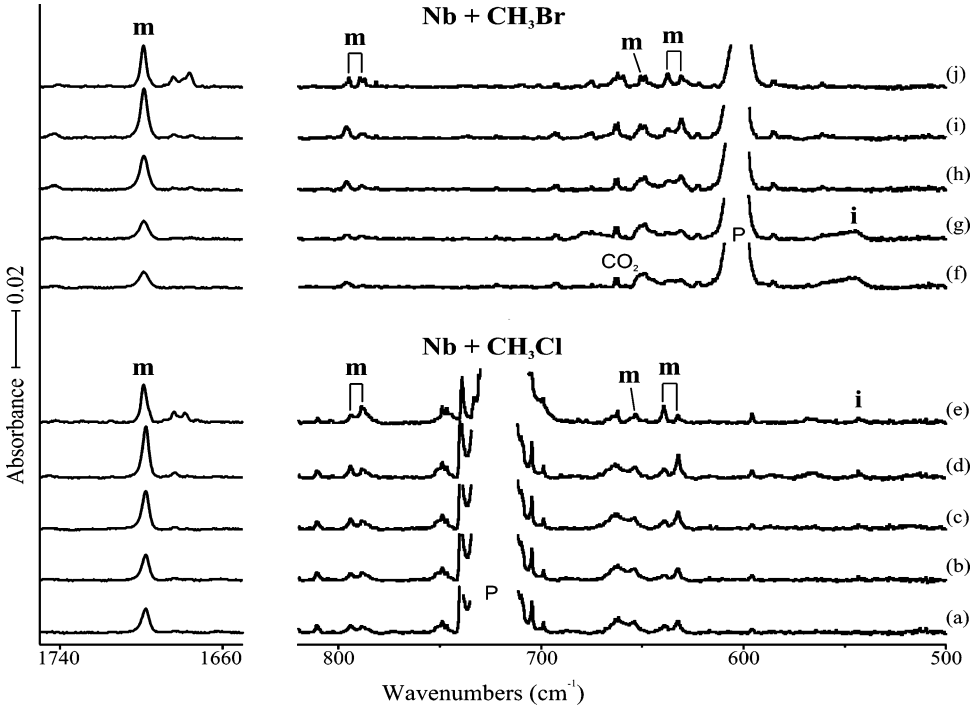

Figure 5. IR spectra in the regions of 1750−1650 and 820−500 cm^{-1} for laser-ablated Nb atoms co-deposited with CH_3Cl (a−e) and CH_3Br (f−j) in excess argon at 8 K and their variation. (a) Nb + 0.5% CH_3Cl in Ar co-deposited for 1 h. (b) After broad-band photolysis with a filter (λ > 420 nm) for 20 min. (c) After broad-band photolysis with a filter (240 < λ < 380 nm) for 20 min. (d) After broad-band photolysis (λ > 220 nm) for 10 min. (e) After annealing to 26 K. (f) Nb + 0.5% CH_3Br in Ar co-deposited for 1 h. (g) After broad-band photolysis with a filter (λ > 420 nm) for 20 min. (h) After broad-band photolysis with a filter (240 < λ < 380 nm) for 20 min. (i) After broad-band photolysis (λ > 220 nm) for 10 min. (j) After annealing to 26 K. **i** and **m** denote the product absorption group. P and CO_2 indicate absorption by precursor and CO_2.

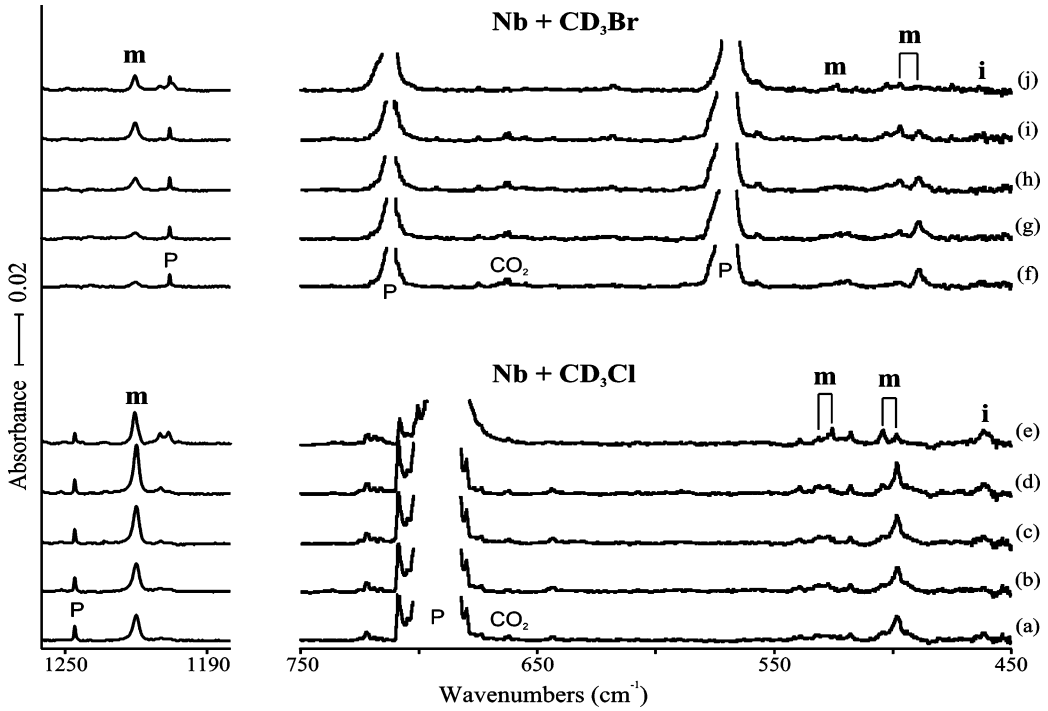

Figure 6. IR spectra in the regions of 1260−1180 and 750−450 cm^{-1} for laser-ablated Nb atoms co-deposited with CD_3Cl (a−e) and CD_3Br (f−j) in excess argon at 8 K and their variation. (a) Nb + 0.5% CD_3Cl in Ar co-deposited for 1 h. (b) After broad-band photolysis with a filter (λ > 420 nm) for 20 min. (c) After broad-band photolysis with a filter (240 < λ < 380 nm) for 20 min. (d) After broad-band photolysis (λ > 220 nm) for 10 min. (e) After annealing to 26 K. (f) Nb + 0.5% CD_3Br in Ar co-deposited for 1 h. (g) After broad-band photolysis with a filter (λ > 420 nm) for 20 min. (h) After broad-band photolysis with a filter (240 < λ < 380 nm) for 20 min. (i) After broad-band photolysis (λ > 220 nm) for 10 min. (j) After annealing to 26 K. **i** and **m** denote the product absorption group. P and CO_2 indicate absorption by precursor and CO_2.

irradiation (b), indicating that they in fact originate from an anionic product.

The distinctive pair of **m** absorptions are observed at 1765.0 and 1759.3 cm^{-1}, and its ^{13}C and deuterium counterparts in similar patterns are found at 1765.1 and 1760.3 cm^{-1} (not shown) and 1263.8 and 1260.3 cm^{-1} (Figure 4), respectively ($^{12}C/^{13}C$ and H/D isotopic ratios of 0.000 and 1.397). The frequencies and isotopic shifts identify the Ta−H stretching

TABLE 5: Frequencies of Product Absorptions Observed from Reactions of Nb and Ta with CH_3Cl and CH_3Br in Excess Argon[a]

	Nb				Ta				
group	CH_3Cl	CD_3Cl	CH_3Br	CD_3Br	CH_3Cl	CD_3Cl	CH_3Br	CD_3Br	description
i	543.2	461.6	544.0	461.7		516.1			C−M str.
m	1697.8	1219.9	1698.7	1220.3	1762.9, **1759.6**	1262.6, **1260.3**	1760.3	1260.9	M−H str.
	794.3		796.4		816.7	729.7	816.6	722.3	C=M str.
	653.7	531.1	651.1, **648.7**	523.4	687.5	543.4			CMH bend
	632.3	498.3	630.8	497.0	660.2, **656.3**	516.1	653.6	512.1	CH_2 wag
a	1547.1	1116.9			1656.3				MH_2 str.

[a] All frequencies are in cm^{-1}. Stronger absorptions are bold. Description gives the major coordinate.

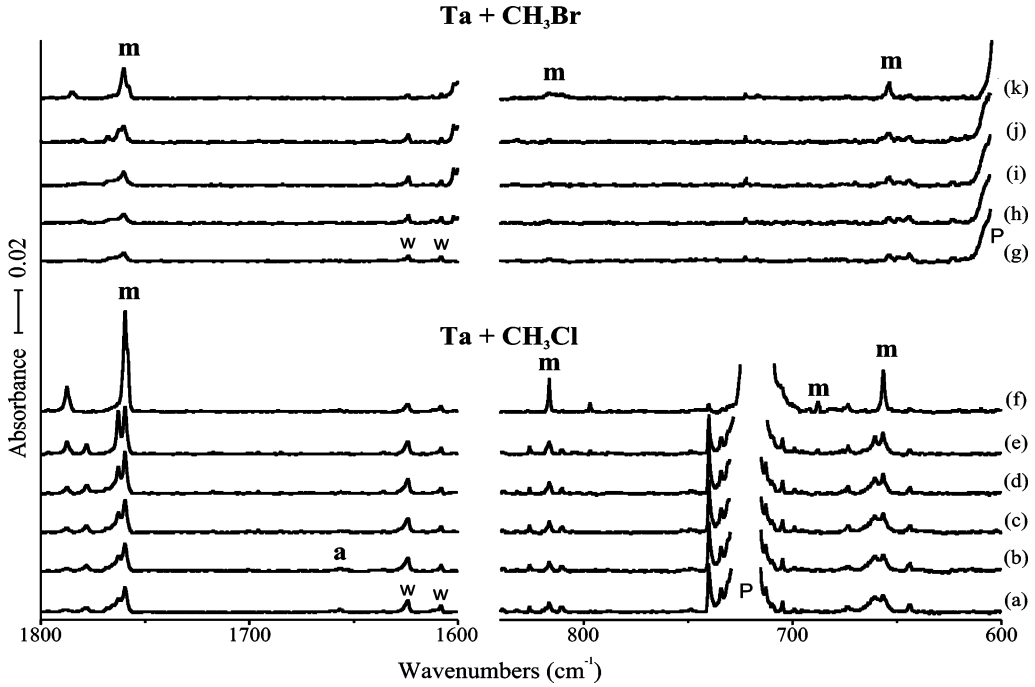

Figure 7. IR spectra in the regions of 1800−1600 and 840−600 cm^{-1} for laser-ablated Ta atoms co-deposited with CH_3Cl (a−f) and CH_3Br (g−k) in excess argon at 8 K and their variation. (a) Ta + 0.5% CH_3Cl in Ar co-deposited for 1 h. (b) After broad-band photolysis with a filter ($\lambda > 420$ nm) for 20 min. (c) After broad-band photolysis with a filter ($240 < \lambda < 380$ nm) for 20 min. (d) After broad-band photolysis ($\lambda > 220$ nm) for 10 min. (e) After annealing to 28 K. (f) After annealing to 44 K. (g) Ta + 0.5% CH_3Br in Ar co-deposited for 1 h. (h) After broad-band photolysis with a filter ($\lambda > 420$ nm) for 20 min. (i) After broad-band photolysis with a filter ($240 < \lambda < 380$ nm) for 20 min. (j) After annealing to 28 K. (k) After annealing to 44 K. **m** and **a** denote the product absorption group. P and w indicate absorption by precursor and water.

absorptions of a reaction product. The hydrogen stretching absorptions of binary tantalum hydrides have been observed in the same frequency region.[30] This indicates that the likely CH_3-TaF intermediate first formed also undergoes α-H transfer to form a methylidene complex, $CH_2=TaHF$.

The **m** absorption at 809.8 cm^{-1} has ^{13}C and D counterparts at 789.1 and 686.6 cm^{-1} ($^{12}C/^{13}C$ and H/D ratios of 1.026 and 1.179), and based upon the frequency and relatively large ^{13}C shift, it is assigned to the C=Ta stretching mode. The absorption at 702.9 cm^{-1}, with its ^{13}C and D counterparts at 701.0 and 660.6 cm^{-1}, is attributed to the Ta−F stretching mode, which is heavily mixed with the in-plane C−Ta−H bending mode. Another **m** absorption at 672.9 cm^{-1} showing ^{13}C and D shifts of −7.3 and −146.2 cm^{-1} ($^{12}C/^{13}C$ and H/D ratios of 1.011 and 1.278) is attributed to the CH_2 wagging mode. The absorption at 621.0 cm^{-1} has its ^{13}C counterpart at 620.3 cm^{-1}, but the deuterium counterpart is not observed, probably due to its low frequency. It is assigned to the C−Ta−H in-plane bending mode. The vibrational characteristics of the observed **m** absorptions all represent the tantalum methylidene complex ($CH_2=TaHF$).

On the red side of the **m** Ta−H stretching absorption at 1765.0 cm^{-1}, two **a** absorptions are observed at 1643.8 and 1608.0 cm^{-1}. The absorption at 1608.0 cm^{-1} is overlapped with a water absorption, which is normally much weaker than another water absorption at 1623.7 cm^{-1}. They increase upon visible irradiation about 30% but decrease upon UV irradiation and annealing. When a trace of CCl_4, which traps electrons from the ablation plume, is included in the reactant mixture, the **a** bands almost completely disappear, indicating that they arise from an anionic product. ^{13}C substitution brings essentially no frequency shifts, but deuteration gives a shift of −451.9 cm^{-1} (the higher frequency component is not observed in the CD_3F spectrum in Figure 4). The large H/D ratio of 1.391 leads to an assignment to the Ta−H stretching mode of the anion.

The two absorptions with about 1:2 ratio in intensity suggest that there are two metal−hydrogen bonds. The observed frequencies are also too high for the anionic tantalum methylidene complex ($CH_2=TaHF^-$(T)), whose Ta−H stretching frequency is expected at about 1580 cm^{-1}. Normally, a higher oxidation state leads to higher stretching frequencies, and the anion, therefore, probably has a carbon−metal triple bond, being consistent with the previous Nb + CH_3F case, which forms $HC\equiv NbH_2F^-$. The Ta−H and Ta−D stretching frequencies are about 56 and 30 cm^{-1} higher than those of $CH\equiv TaH_3^-$ prepared previously.[15] The **a** absorption at 913.3 cm^{-1} has its ^{13}C

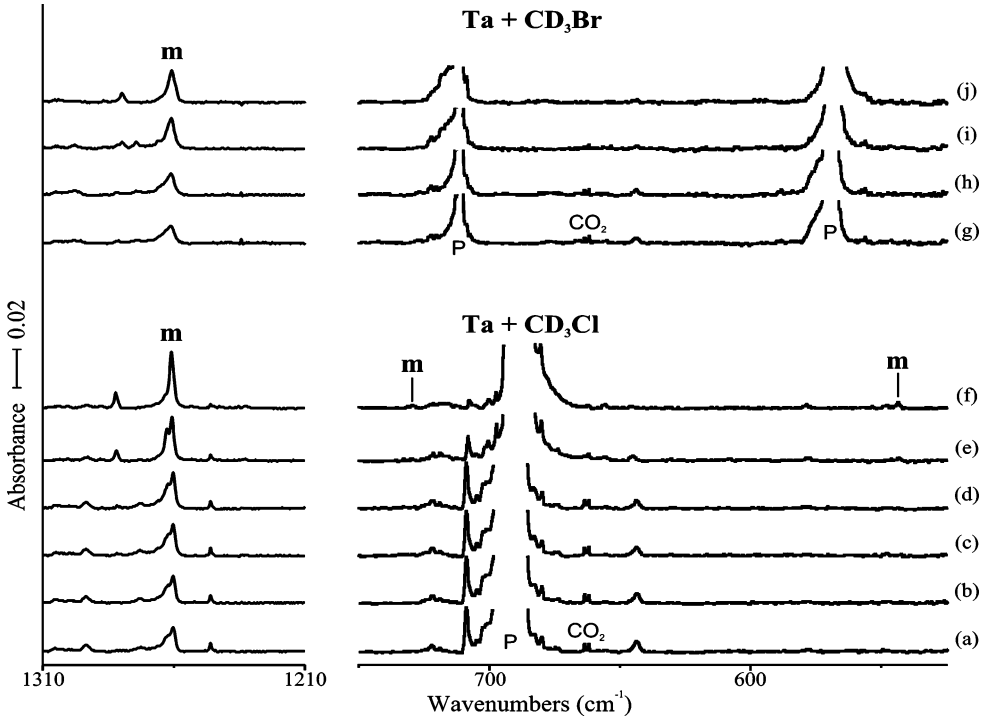

Figure 8. IR spectra in the regions of 1310−1210 and 800−530 cm^{-1} for laser-ablated Ta atoms co-deposited with CD_3Cl (a−f) and CD_3Br (g−j) in excess argon at 8 K and their variation. (a) Ta + 0.5% CD_3Cl in Ar co-deposited for 1 h. (b) After broad-band photolysis with a filter (λ > 420 nm) for 20 min. (c) After broad-band photolysis with a filter (240 < λ < 380 nm) for 20 min. (d) After broad-band photolysis (λ > 220 nm) for 10 min. (e) After annealing to 28 K. (f) After annealing to 44 K. (g) Ta + 0.5% CD_3Br in Ar co-deposited for 1 h. (h) After broad-band photolysis with a filter (240 < λ < 380 nm) for 20 min. (i) After annealing to 36 K. (j) After annealing to 44 K. **m** denotes the product absorption group. P and CO_2 indicate absorption by precursor and CO_2.

counterpart at 883.4 cm^{-1} (not shown). The deuterium counterpart is very weak at 869.2 cm^{-1}. The absorption intensities of the deuterium insertion complexes are relatively lower as mentioned above. On the basis of the frequency and relatively large ^{13}C shift, the band is attributed to the C≡Ta stretching mode.

On the further red side, the absorption at 637.5 cm^{-1} has its ^{13}C counterparts at 636.4 cm^{-1} ($^{12}C/^{13}C$ H/D ratio of 1.002) but the D counterpart is not observed probably due to its low frequency. It is assigned to the TaH_2 bending mode. The **a** absorption at 612.0 cm^{-1} has ^{13}C and D counterparts at 611.4 and 579.8 cm^{-1} ($^{12}C/^{13}C$ and H/D ratios of 1.001 and 1.056) and is assigned to the Ta−F stretching mode. Another **a** absorption at 578.8 cm^{-1} shows ^{13}C shifts of −4.2 cm^{-1} and is assigned to the MCH bending mode while the deuterium counterpart is not observed. The vibrational characteristics of the **a** absorptions show that $HC{\equiv}TaH_2F^-$ is formed in the reaction of Ta + CH_3F, parallel to the case of Nb + CH_3F. The predicted frequencies for group 5 anionic methylidyne ($CH{\equiv}MH_2F^-$) are listed in Table 4.

On the other hand, unlike the cases of V and Nb, the C−F insertion complex, CH_3−TaF, is not identified in the spectra, suggesting that CH_3−TaF, after formed first in the reaction of Ta + CH_3F, converts to another higher oxidation-state complex via α-hydrogen migration.

Nb + CH_3X. The formation of CH_3−NbF, CH_2═NbHF, and $CH{\equiv}NbH_2F^-$ has recently been reported, and $CH{\equiv}NbH_2F^-$ is believed to be the first anionic group 5 metal methylidyne complex.[14] In an effort to understand the ligand effects, reactions of laser-ablated niobium and tantalum atoms with CH_3Cl and CH_3Br are carried out. Figure 5 shows the IR spectra in the regions of 1750−1650 and 820−500 cm^{-1} from the products of Nb reactions with CH_3Cl and CH_3Br, where CH_3Cl and CH_3Br give similar product absorptions. The absorptions marked "**m**" increase about 20% and 80% upon visible and UV irradiations, respectively, and increase another 50% upon full arc irradiation (λ > 220 nm). The Nb−Cl and Nb−Br stretching frequencies are below our observation limit, and other **i** absorptions are mostly too weak to be observed (Figures 5 and 6).

The spectra are relatively simple, and the strongest absorptions marked "**m**" are observed at ∼1700 cm^{-1}. The absorptions at 1697.8 and 1698.7 cm^{-1} from CH_3Cl and CH_3Br have their deuterium counterparts at 1219.9 and 1220.3 cm^{-1} (H/D ratios of both 1.392) in Figure 6, respectively. The Nb−H stretching absorptions indicate formation of CH_2═NbHX and show essentially no variation in the Nb−H stretching frequency with halogen size as listed in Tables 1 and 5. Two similar **m** absorptions are observed at 794.3 and 796.4 cm^{-1}. While the deuterium counterparts are probably overlapped by precursor absorptions, based upon the frequency and consistency with previous studies, they are assigned to the C═Nb stretching modes of CH_2═NbHCl and CH_2═NbHBr, respectively. The **m** absorptions at 653.7 and 648.7 cm^{-1} have their deuterium counterparts at 531.1 and 523.4 cm^{-1} (H/D ratios of 1.231 and 1.239) and are attributed to the CNbH bending modes. The **m** absorptions at 632.3 and 630.8 cm^{-1} and their D counterparts at 498.3 and 497.0 cm^{-1} (H/D ratios of both 1.269) are assigned to the CH_2 wagging modes of CH_2═NbHCl and CH_2═NbHBr, respectively.

Other than **m** absorptions, the observed product bands are very weak and only tentatively assigned. A weak absorption at 1547.1 cm^{-1} marked "**a**" and its deuterium counterpart at 1116.9 cm^{-1} (not shown) decrease and completely disappear upon UV and full arc irradiation, respectively. On the basis of previous results of Nb + CH_3F reactions, they are assigned to the NbH_2 antisymmetric stretching mode of $CH{\equiv}NbH_2Cl^-$; however, their bromine counterparts are not observed. Clearly, the anionic

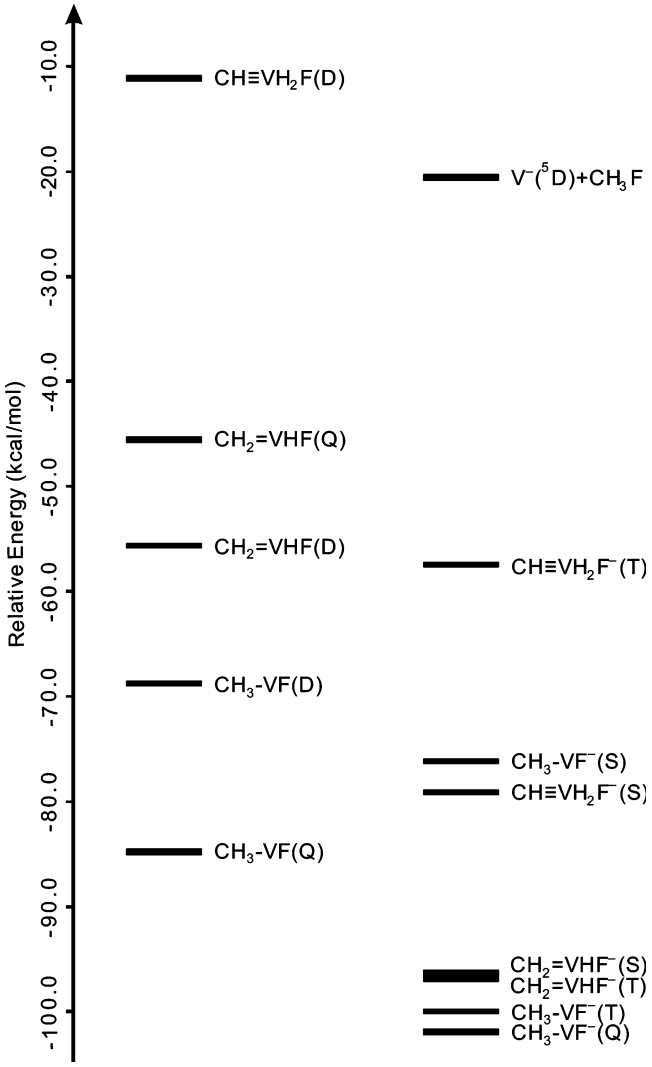

Figure 9. Energies calculated using the B3LYP density functional for neutral and anionic products relative to $V(^4F) + CH_3F$. Note that $CH_3-VF(Q)$ and $CH_2=VHF(D)$ are the most stable ones among the plausible neutral primary products, whereas $CH\equiv VH_2F$ is too high in energy. Also note that $CH\equiv VH_3^-(S)$ is not the most stable among the plausible anionic products, but the single and double bonded insertion complexes are the most stable instead. S, D, T, and Q denote singlet, doublet, triplet, and quartet or quintet states.

species becomes less favored with increasing halogen size. Absorptions at 543.2 and 544.0 cm^{-1} marked "**i**" from CH_3Cl and CH_3Br have their D counterparts at 461.6 and 461.7 cm^{-1}, and they are assigned to predominately C−Nb stretching modes, which are normally much weaker than the Nb−X stretching band.

Ta + CH_3X. Shown in Figure 7 are the IR spectra in the regions of 1800−1600 and 750−530 cm^{-1} observed from the product of Ta reactions with CH_3Cl and CH_3Br. The observed absorptions mostly originate from the methylidene complex, $CH_2=TaHX$. The **m** absorptions increase about 10, 20, and 35% upon visible, UV, and full arc irradiations, respectively, and more interestingly they increase dramatically in the process of annealing (up to 300%). The dramatic increases in intensity upon annealing are also evident in the spectra of deuterated isotopomers shown in Figure 8. A similar increase in intensity in annealing is not observed in the Ta + CH_3F system (Figures 3 and 4). Figures 7 and 8 also show that CH_3Br is less reactive with Ta than CH_3Cl.

The strong **m** absorptions at 1759.6 and 1760.3 cm^{-1} from CH_3Cl and CH_3Br have their deuterium counterparts at 1260.3 and 1260.9 cm^{-1} (H/D ratios of both 1.396). The frequencies of the Ta−H stretching absorptions slightly decrease with increasing halogen size. On the blue side of the absorptions, weaker absorptions appear particularly in the process of annealing at 1787.5 and 1784.8 cm^{-1} from CH_3Cl and CH_3Br, respectively. They probably originate from a weakly bound complex of $CH_2=TaHX$ and CH_3X. The **m** absorptions at 816.7 and 816.6 cm^{-1} from CH_3Cl and CH_3Br and the weak absorption at 729.7 cm^{-1} from CD_3Cl are attributed to the C=Ta stretching modes of $CH_2=TaHX$.

In the further low-frequency region, the weak **m** absorption at 687.5 from CH_3Cl has its deuterium counterpart at 543.4 cm^{-1} and is assigned to the C−Ta−H in-plane bending mode (the corresponding absorptions are not observed from CH_3Br). The absorption at 656.3 and 653.6 cm^{-1} from CH_3Cl and CH_3Br have their D counterparts at 516.1 and 512.1 cm^{-1} (not shown), respectively. They are attributed to the CH_2 wagging modes.

A weak absorption marked "**a**" is observed at 1656.3 cm^{-1} only in the Ta + CH_3Cl spectra, which decrease and completely disappear upon UV and full arc photolysis. We tentatively assign the band to the antisymmetric hydrogen stretching mode of $CH\equiv TaH_2Cl^-$ on the basis of its behavior upon photolysis and the frequency consistent with that of $CH\equiv TaH_2F^-$ described above. Parallel to the case of Nb + CH_3X, the anionic species become less favorable with increasing halogen size. Absorptions marked "**i**" are not observed like in the case of Ta + CH_3F.

Discussion

V + CH_3F. Reactions of Ti and Cr with CH_3F have been studied previously.[1,13] Both metals readily form C−F insertion complexes in the reaction with CH_3F and Ti also produces the higher-order complex, $(CH_3)_2TiF_2$. Upon UV photolysis, Ti forms the methylidene complex ($CH_2=TiHF$) via α-hydrogen migration, and upon subsequent visible photolysis, the Ti methylidene converts back to CH_3-TiF. The interconversions by UV and visible irradiations consist of a persistent photoreversible system.[1] On the other hand, Cr does not form a methylidene complex either during reaction with CH_3F or on subsequent irradiation.[13] Our DFT calculations show that the C−F insertion complex with Cr is far more stable than the higher oxidation-state complexes, and as a result, CH_3-CrF is highly favored over $CH_2=CrHF$ and $CH\equiv CrH_2F$.

The reaction of V with CH_3F is considered a good test regarding the formation of a higher oxidation-state complex, and CH_3-VF and $CH_2=VHF$ are identified in the IR spectra shown in Figures 1 and 2. This is compared with the case of V + CH_4, where only the single insertion complex is formed. In reaction of V with CH_3F, CH_3-VF is the primary product and more complex is formed in visible photolysis afterward. On the other hand, CH_3-VF converts to $CH_2=VHF$ in UV photolysis via α-hydrogen migration and $CH_2=VHF$ converts back to CH_3-VF upon visible photolysis as shown in Figures 1 and 2, consisting of a persistent photoreversible system. Similar to titanium, vanadium forms $CH_2=VHF$: however, the higher-order complex, $(CH_3)_2VF_2$, is not identified in the spectra. While Nb and Ta form anionic methylidyne complexes, $CH\equiv MH_3^-$ and $CH\equiv MH_2X^-$,[14,15] the analogous product is not identified in the V + CH_3F spectra.

Figure 9 shows the energies of the plausible reaction products relative to $V(^4F) + CH_3F$. Clearly, $CH_3-VF(Q)$ is the most stable neutral product and $CH_2=VHF(D)$ is 28.9 kcal/mol higher in energy. This is consistent with the result that CH_3-VF is

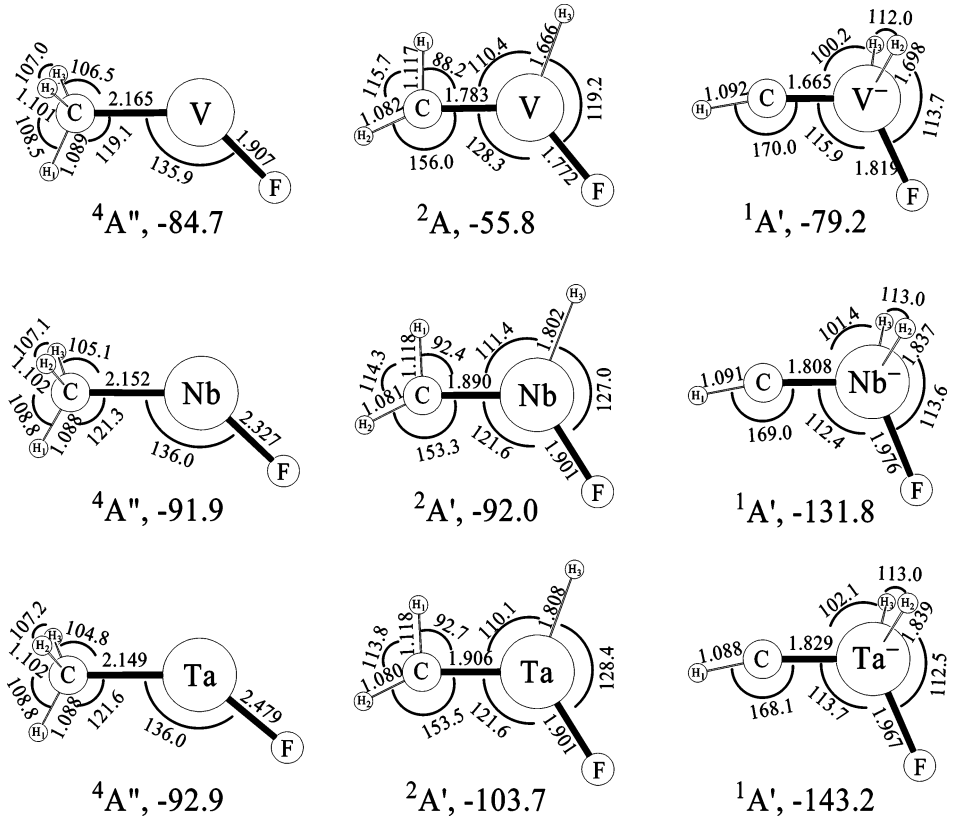

Figure 10. Optimized molecular structures of the methyl, methylidene, and anionic methylidyne complexes of group 5 transition metals with CH_3F calculated using B3LYP and the 6-311++G(3df,3pd) basis set. All electron basis and SDD pseudopotential and basis are used for V, Nb, and Ta, respectively. The bond lengths and angles are in angstroms and degrees. The electronic states and energies in kcal/mol relative to the metal and CH_3F are shown below the structure.

the primary reaction product and $CH_2{=}VHF$ is formed from the single-bonded insertion complex in UV photolysis afterward as shown in Figures 1 and 2. It is on the other hand compared with the V + CH_4 case, where $CH_2{=}VH_2$ is 33.8 kcal/mol higher than $CH_3{-}VH$. The V methylidene hydride complex is not identified even after UV photolysis. The methylidyne complex ($CH{\equiv}VH_2F$) is undoubtedly too high in energy relative to $CH_3{-}VF$ and $CH_2{=}VHF$. Although no anionic species is identified in reaction of V + CH_3F, the energies of the plausible anionic products are also shown in Figure 9. Unlike the cases of Nb and Ta, $CH{\equiv}VH_2F^-$(S) is not the most stable one, but even among the anionic species, the single-bonded insertion complex is the most stable product instead.

The predicted structures of methyl, methylidene, and methylidyne complexes of group 5 metals with CH_3F using B3LYP/6-311++G(3df,3pd) are shown in Figure 10. It is notable that the methylidene complexes are all agostically distorted. Previous studies of group 4 methylidene complexes show that distortion becomes less serious going down the column.[1,3,8,9] Similarly, $CH_2{=}VHF$ has the most distorted structure ($\angle HCV = 88.2°$) among the group 5 methylidene complexes. It is also interesting that the group 5 metal methylidene complexes are more agostically distorted than the group 4 metal complexes.[1,9] Previous studies indicate that more electron density in the carbon−metal bond in the methylidene complex generally increases the agostic distortion and shortens the length of the double bond.[1,3,8,9] The group 5 metal methylidene complexes probably can afford more electron density to the carbon−metal double bond than the group 4 metal counterpart because they have one more electron in the valence shell. Previous studies also show that the group 6 metal (Mo and W) methylidenes in the triplet ground states have even more agostically distorted structures.[13]

Ta + CH_3F. The frequencies of the Ta products are higher than those of the Nb products, due to the larger relativistic contraction for Ta predicted by Pyykko et al.[31] The primary reaction products of Ta with CH_3F are $CH_2{=}TaHF$ and $CH{\equiv}TaH_2F^-$ as shown in Figures 3 and 4, whereas the C−F insertion complex ($CH_3{-}TaF$) is not identified. In previous studies of third-row transition metals (Hf and W), the single insertion complexes ($CH_3{-}MF$ and $CH_3{-}MH$) are also not identified in the IR spectra, and this is explained by the lack of stability of the single bonded insertion complexes relative to the higher oxidation-state complexes.

It should be remembered that the primary reaction products with Ti, V, and Cr are the single-bonded insertion complexes ($CH_3{-}MH$, and $CH_3{-}MX$)[1−3,12,13,15] and the methylidene complexes are mostly produced by photolysis afterward. On the other hand, the second-row transition metals produce the three possible complexes in reactions with methane and methyl halides, indicating that, even after the single insertion, a considerable portion of the first formed product undergoes rearrangement to the higher oxidation-state complexes.[5−8,10,11] In the case of the third-row transition metals, the first insertion complexes produced originally all proceed for further reactions to form the higher oxidation-state complexes, leaving no single-bonded insertion complexes.[4,9,12,13]

These results for group 4, 5, and 6 metals show that higher oxidation-state complexes become relatively more stable than the lower oxidation-state complexes with heavier metal atoms. Calculation results also demonstrate this tendency. The energies

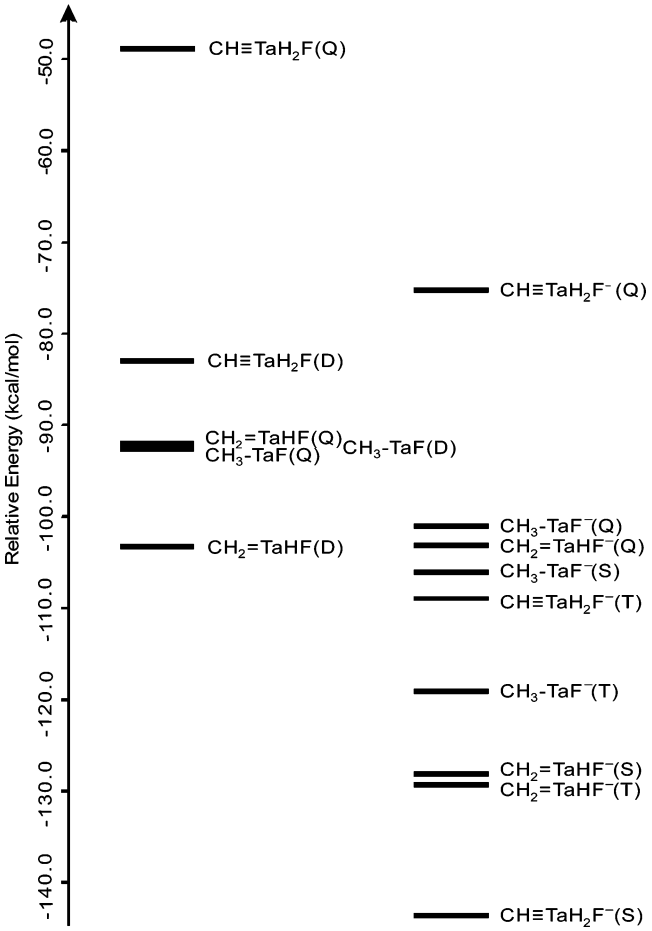

Figure 11. Energies calculated using the B3LYP density functional for neutral and anionic products relative to Ta(^{4}F) + CH_3F. Note that $CH_2=TaHF(D)$ is the most stable one among the plausible neutral primary products, whereas $CH_3-VF(Q)$ is 11 kcal higher in energy. Also note that $CH\equiv TaH_3^-(S)$ is clearly the most stable species among the plausible anionic products, which is 40 kcal/mol lower in energy than the most stable neutral species. $CH_3-TaF(Q)$, $CH_2=TaHF(Q)$, and $CH_3-TaF(D)$ have almost the same energies. S, D, T, and Q denote singlet, doublet, triplet, and quartet or quintet states.

of the plausible reaction products of Ta with CH_3F relative to Ta(^{4}F) + CH_3F are shown in Figure 11, where among the neutral species, $CH_2=TaHF(D)$ is 10.8 kcal/mol more stable than $CH_3-TaF(Q)$. This is in line with the result that $CH_2=TaHF$ is the primary neutral product in the reaction of Ta + CH_3F and the single and triple insertion complexes are not identified in the spectra. Among the anionic species, $CH\equiv TaH_2F^-$ is evidently the most stable product, which is consistent with the result that it is the only anionic product identified in the reaction of Ta + CH_3F. Figure 11 also shows that $CH\equiv TaH_2F^-$ is 40 kcal/mol more stable than the most stable neutral species, whereas in the V + CH_3F system, the most stable anionic species is only 19.3 kcal/mol more stable than $CH_3-VF(Q)$ and no anionic product is identified.

Upon gaining an extra electron, the tantalum atom becomes isoelectronic to the tungsten atom, which readily produces the methylidyne complexes. Formation of niobium anionic methylidyne complexes, $CH\equiv NbH_2F^-$ and $CH\equiv NbH_3^-$, is reported in recent studies of niobium reactions with CH_3F and CH_4, respectively.[14,15] $CH\equiv TaH_3^-$ is also prepared in the reaction of tantalum atoms with CH_4.[15] Along with these first anionic group 5 metal methylidyne complexes, $CH\equiv TaH_2F^-$ is also prepared in this study. Formation of the anionic methylidyne complexes, therefore, can now be considered as a general property of the heavy group 5 metals.

Figure 3 also shows that the fast decrease of $CH\equiv TaH_2F^-$ upon UV irradiation is accompanied with a large increase of $CH_2=TaHF$. After losing an electron upon UV photolysis, the methylidyne becomes very unstable as shown in Figure 9 and, therefore, eventually converts to the methylidene complex.

Nb + CH_3X. The reactions of Nb with CH_3Cl and CH_3Br are performed to understand the ligand effects on the insertion complexes. Similar studies with group 4 metals show that the agostic distortion of the methylidene complex increases with increasing halogen size.[3,8] Calculations indicate that the lower electronegativity of the heavier halogen atom allows more electron density to remain in the carbon−metal double bond, leading to a more agostic distortion. The observed carbon−metal stretching frequencies and calculated bond lengths also affirm the stronger double bond with increasing halogen size.[3,8]

Tables 1 and 5 list the observed frequencies and Tables 9−11 show the molecular parameters of the single-, double-, and triple-bonded complexes examined in this study. Figure 12 illustrates the predicted structures of Nb and Ta methylidene complexes with varying halogen size, where the methylidene complexes have planar structures except $CH_2=NbHBr$ with C_1 (but near planar) structure. It is notable that they become more agostically distorted with increasing halogen size, similar to the case of group 4 metal methylidenes.[3,8] The carbon−metal bond length decreases and the stretching frequency increases with increasing halogen size while the Nb−H stretching frequency slightly decreases. Parallel to the case of group 4 metal methylidenes,

TABLE 6: Calculated Fundamental Frequencies of CH_3-MCl and CH_3-MBr (M = Nb, Ta) Isotopomers in the Ground $^4A''$ Electronic State[a]

approximate description	Nb + CH_3Cl			Nb + CH_3Br			Ta + CH_3Cl			Ta + CH_3Br		
	CH_3-NbCl	int.	CD_3-NbCl	CH_3-NbBr	int.	CD_3-NbBr	CH_3-TaCl	int.	CD_3-TaCl	CH_3-TaBr	int.	CD_3-TaBr
A′ CH_3 str.	3120.2	1	2302.6	3121.3	0	2303.5	3108.0	2	2293.3	3107.6	0	2293.2
A′ CH_3 str.	2934.5	4	2108.2	2933.3	5	2107.2	2948.8	2	2118.9	2949.9	3	2119.5
A′ CH_3 bend	1399.0	5	1016.5	1397.7	5	1015.7	1402.6	20	1017.7	1401.4	8	1016.8
A′ CH_3 deform	1156.2	9	912.9	1153.8	8	911.5	1172.0	6	924.9	1171.3	17	925.0
A′ C−M str.	565.3	34	485.9	564.5	37	485.2	550.6	28	473.5	547.6	30	471.3
A′ M−X str.	391.7	106	381.8	360.4	64	300.2	388.4	17	364.5	379.8	40	301.3
A′ CH_3 rock	347.0	6	285.2	261.3	20	249.9	352.5	24	296.0	238.7	23	235.8
A′ CMX bend	103.8	1	94.2	90.4	0	81.1	94.3	1	86.4	83.0	0	74.8
A″ CH_3 str.	2987.8	5	2205.0	2987.2	5	2204.6	3002.6	31	2216.0	3004.4	3	2217.4
A″ CH_3 bend	1414.6	4	1026.9	1413.7	5	1026.3	1411.0	25	1023.6	1410.0	6	1023.0
A″ CH_2 rock	341.0	3	254.2	335.8	3	250.7	377.2	7	280.9	376.2	3	280.1
A″ CH_3 distort	99.5	0	72.8	99.5	0	72.5	65.7	2	48.8	61.0	0	45.3

[a] Calculated at the level of B3LYP/6-311++G(3df, 3pd), and SDD core potential and basis set are used for Nb and Ta. Frequencies and intensities are in cm^{-1} and km/mol. Intensities are calculated values for the product of CH_3Cl or CH_3Br.

TABLE 7: Calculated Fundamental Frequencies of CH_2═MHCl and CH_2═MHBr (M = Nb, Ta) Isotopomers in the Ground ^1A Electronic State[a]

approximate description	Nb + CH_3Cl			Nb + CH_3Br			Ta + CH_3Cl			Ta + CH_3Br		
	CH_2═NbHCl	int.	CD_2═NbHCl	CH_2═NbHBr	int.	CD_2═NbHBr	CH_2═TaHCl	int.	CD_2═TaHCl	CH_2−TaHBr	int.	CD_2═TaHBr
A′ C−H str.	3210.6	4	2377.5	3210.6	5	2377.5	3224.9	4	2388.1	3224.2	5	2387.6
A′ C−H str.	2791.2	4	2031.4	2776.7	5	2020.7	2781.1	6	2025.1	2773.5	6	2019.4
A′ M−H str.	1755.8	291	1249.2	1755.1	306	1248.7	1805.4	252	1280.9	1803.8	264	1279.7
A′ CH_2 scis.	1338.9	20	1047.7	1334.0	20	1046.7	1340.8	21	1045.8	1339.7	21	1044.5
A′ C═M str.	819.4	70	721.1	820.5	70	723.3	823.1	54	724.0	823.0	56	724.3
A′ CMH bend	725.7	19	553.8	719.6	15	547.3	695.8	17	523.2	693.1	12	518.9
A′ CH_2 rock	439.5	1	323.4	439.2	3	326.4	440.3	1	326.6	438.7	6	328.6
A′ M−X str.	382.4	55	382.1	274.5	29	267.8	371.0	53	372.4	251.5	24	249.1
A′ CMX bend	147.5	2	133.0	144.0	11	124.6	141.4	1	126.9	126.2	1	112.5
A″ CH_2 wag	696.7	80	545.1	687.2	80	536.8	696.9	71	544.4	691.7	69	540.1
A″ CH_2 twist	414.2	7	294.2	396.0	11	283.3	394.8	9	280.5	366.5	10	260.4
A″ MH oop bend	39.2	45	28.1	64.0	31	51.0	137.1	19	99.8	110.9	17	81.2

[a] Frequencies and intensities computed at the level of B3LYP/6-311++G(3df, 3pd)SDD, and SDD core potential and basis set are used for Nb and Ta. Frequencies and intensities are in cm^{-1} and km/mol. Intensities are calculated values for the product of CH_3Cl and CH_3Br.

TABLE 8: Calculated Fundamental Frequencies of CH≡MH_2Cl^- and CH≡MH_2Br^- (M = Nb, Ta) Isotopomers in the Ground $^1A'$ Electronic State[a]

approximate description	Nb + CH_3Cl			Nb + CH_3Br			Ta + CH_3Cl			Ta + CH_3Br		
	CH≡NbH_2Cl^-	int.	CD≡NbD_2Cl^-	CH≡NbH_2Br^-	int.	CD≡NbD_2Br^-	CH≡TaH_2Cl^-	int.	CD≡TaD_2Cl^-	CH≡TaH_2Br^-	int.	CD≡TaD_2Br^-
A′ C−H str.	3123.9	13	2318.1	3128.1	12	2319.9	3146.4	12	2333.4	3149.5	11	2335.9
A′ MH_2 str.	1642.9	436	1167.6	1648.3	446	1171.4	1693.7	406	1201.4	1700.1	415	1205.9
A′ C≡M str.	958.1	125	916.7	960.3	120	918.6	945.9	122	903.1	948.2	120	905.0
A′ MH_2 wag	636.2	30	491.4	640.4	38	496.6	643.8	88	478.9	645.5	71	484.2
A′ MH_2 scis.	597.3	265	433.1	593.1	249	426.0	608.3	179	453.2	615.6	192	453.7
A′ MCH bend	541.6	23	400.2	546.4	16	397.3	564.2	17	409.9	566.3	12	406.7
A′ M−X str.	301.4	40	290.4	218.5	18	212.6	294.0	48	288.2	198.6	23	195.9
A′ CMX bend	162.9	3	151.1	141.8	2	131.6	156.7	6	145.7	138.2	4	128.0
A″ MH_2 str.	1610.6	595	1150.8	1616.6	570	1154.9	1660.7	512	1180.9	1668.5	484	1186.3
A″ CH o−o-p bend	667.1	10	529.7	671.0	9	532.2	645.2	40	510.2	645.5	35	510.4
A″ MH_2 twist	516.1	94	365.6	521.2	90	369.1	540.6	76	383.2	544.8	76	385.7
A″ MH_2 rock	278.4	16	206.6	260.6	14	192.7	270.8	19	200.1	263.2	17	192.4

[a] B3LYP/6-311++G(3df,3pd)/SDD level. Frequencies and intensities are in cm^{-1} and km/mol. Intensities are calculated values for the product of CH_3Cl and CH_3Br.

TABLE 9: Geometrical Parameters and Physical Constants Calculated for CH_3−MX Complexes[a]

parameters	CH_3−VF	CH_3−NbF	CH_3−NbCl	CH_3−NbBr	CH_3−TaF	CH_3−TaCl	CH_3−TaBr
$r(C-H_1)$	1.090	1.089	1.088	1.088	1.089	1.089	1.089
$r(C-H_2)$	1.098	1.101	1.102	1.102	1.100	1.101	1.101
r(C−M)	2.073	2.165	2.152	2.149	2.171	2.161	2.158
r(M−X)	1.786	1.907	2.327	2.479	1.910	2.332	2.487
$\angle H_1CH_2$	108.1	108.5	108.8	108.8	108.2	108.4	108.5
$\angle H_2CH_3$	107.5	107.0	107.1	107.2	106.6	107.0	107.0
∠CMX	134.0	135.9	136.0	136.0	140.0	141.0	141.4
$\angle H_1CM$	115.2	119.1	121.3	121.6	118.2	118.7	118.7
$\angle H_2CM$	108.8	106.5	105.1	104.8	107.5	106.9	106.8
$\Phi(H_1CMH_2)$	121.6	123.2	123.6	123.6	122.8	122.9	122.9
$\Phi(H_1CMX)$	0.0	0.0	0.0	0.0	0.0	0.0	0.0
mol. sym.	C_s	C_s	C_s	C_s	C_s	C_s	C_s
q(C)[b]	−0.39	−0.92	−0.99	−0.97	−0.74	−0.81	−0.79
$q(H_1)$[b]	0.01	0.03	0.02	0.03	0.02	0.03	0.02
$q(H_2)$[b]	0.01	0.06	0.08	0.09	0.05	0.06	0.06
$q(H_3)$[b]	0.01	0.06	0.08	0.09	0.05	0.06	0.06
q(M)[b]	0.87	1.33	1.63	1.37	1.08	1.43	1.17
q(X)[b]	−0.51	−0.57	−0.82	−0.60	−0.47	−0.78	−0.53
μ[c]	2.47	1.96	2.48	2.55	1.71	2.06	2.12
state[d]	$^4A''$	$^4A''$	$^4A''$	$^4A''$	$^4A''$	$^4A''$	$^4A''$
ΔE[e]	84.7	91.9	86.4	85.7	92.9	85.5	84.0

[a] Bond lengths and angles are in angstroms and degrees. Calculated using the 6-311++G(3df, 3pd) basis set and SDD core potential and basis set for Nb and Ta. [b] Mulliken atomic charge. [c] Molecular dipole moment in D. [d] Electronic state. [e] Binding energies in kcal/mol.

these results indicate the stronger carbon−metal double bond with the larger halogen, which in turn causes more distortion of the CH_2 group.

According to Scherer and McGrady, the agostic interaction results from delocalization of the carbon−metal bonding electrons rather than the donation of electron density located on the alkyl substituent into a vacant orbital of the electron deficient metal atom.[18] Therefore, agostic interaction includes not just the inclination of the C−H bond toward the d^0-metal atom but rearrangement of the molecular structure around the carbon−metal bond. The present results show that the ligand can affect considerably the agostic interaction of the methylidene complex, probably by causing variation in electron density in the carbon−metal bond.

The previous and present results indicate that the relative production yield for the anionic methylidyne complex

TABLE 10: Geometrical Parameters and Physical Constants Calculated for $CH_2=MHX$ Complexes[a]

parameters	$CH_2=VHF$	$CH_2=NbHF$	$CH_2=NbHCl$	$CH_2=NbHBr$	$CH_2=TaHF$	$CH_2=TaHCl$	$CH_2=TaHBr$
$r(C-H_1)$	1.117	1.118	1.123	1.125	1.118	1.125	1.126
$r(C-H_2)$	1.082	1.081	1.081	1.081	1.080	1.080	1.080
$r(C-M)$	1.783	1.890	1.881	1.878	1.906	1.897	1.895
$r(M-H_3)$	1.666	1.802	1.797	1.794	1.808	1.802	1.801
$r(M-X)$	1.772	1.901	2.319	2.468	1.901	2.318	2.470
$r(M\cdots H)$	2.075	2.236	2.172	2.154	2.254	2.183	2.174
$\angle H_1CH_2$	115.7	114.3	114.7	114.8	113.8	114.0	114.0
$\angle CMX$	128.3	121.6	121.9	120.6	121.6	122.5	122.4
$\angle CMH_3$	110.4	111.4	110.8	110.1	110.0	108.8	108.6
$\angle H_3MX$	119.2	127.0	127.3	126.4	128.4	128.7	129.0
$\angle H_1CM$	88.3	92.4	88.9	87.9	92.7	88.7	88.2
$\angle H_2CM$	156.0	153.3	156.3	157.0	153.5	157.3	157.8
$\Phi(H_1CMH_3)$	6.5	0.0	0.0	3.7	0.0	0.0	0.0
$\Phi(H_1CMX)$	169.9	180.0	180.0	165.8	180.0	180.0	180.0
mol. sym.	C_1	C_s	C_s	C_1	C_s	C_s	C_s
$Q(C)^b$	−0.57	−0.78	−0.77	−0.80	−0.56	−0.13	−0.55
$Q(H_1)^b$	0.10	0.02	0.00	0.01	0.01	0.00	−0.01
$Q(H_2)^b$	0.07	0.00	0.00	−0.01	0.07	0.00	0.08
$Q(H_3)^b$	−0.22	−0.43	−0.45	−0.42	−0.31	−0.03	−0.32
$Q(M)^b$	1.13	1.80	2.02	1.75	1.24	1.19	1.30
$Q(X)^b$	−0.51	−0.61	−0.79	−0.54	−0.45	−0.03	−0.49
μ^c	1.90	1.05	1.25	1.37	0.73	0.78	0.73
state[d]	^2A	$^2A'$	$^2A'$	^2A	$^2A'$	$^2A'$	$^2A'$
ΔE^e	55.8	92.0	85.6	84.6	103.7	95.3	93.5

[a] Bond lengths and angles are in angstroms and degrees. Calculated with the B3LYP/6-311++G(3df, 3pd) basis set and SDD core potential and basis set for Nb and Ta. [b] Mulliken atomic charge. [c] Molecular dipole moment in D. [d] Electronic state. [e] Binding energies in kcal/mol.

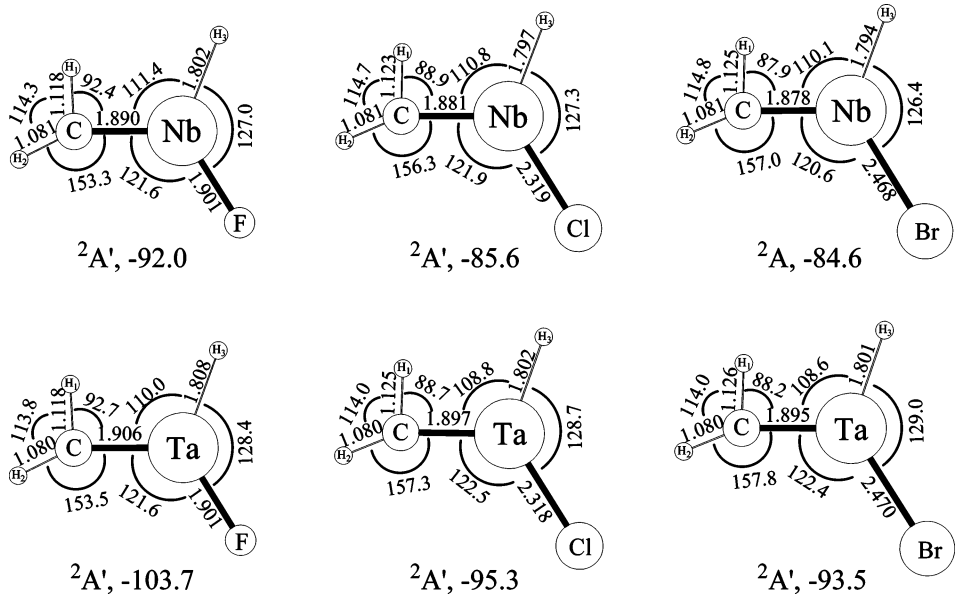

Figure 12. Optimized molecular structures of the methylidene complexes of Nb and Ta with CH_3X calculated using B3LYP and the 6-311++G-(3df,3pd) basis set. The SDD pseudopotential and basis are used for Nb and Ta. The bond lengths and angles are in angstroms and degrees. The electronic states and energies in kcal/mol relative to the metal and CH_3F are shown below the structure.

($CH\equiv NbH_2X^-$) decreases in the order of X = H, F, Cl, and Br. However, the binding energies for the anionic methylidyne complexes are comparable regardless of the halogen size as listed in Table 11, and they are the most stable ones among the plausible anionic products. While there is no clear explanation for this tendency, it should be noted at this point that CCl_4 and CBr_4 are often used to capture electrons produced in the process of laser ablation.[15,24] It is, therefore, highly possible that extra CH_3Cl and CH_3Br reagent molecules also trap electrons and deprive the reaction products from electron capture to form an anion.

Ta + CH_3X. The IR spectra in Figures 7 and 8 show a dramatic increase of the methylidene complexes in the process of annealing. Thermally initiated formation of the methylidene complex in such a magnitude is unprecedented in matrix studies of transition-metal reactions with methane and methyl halides. In the reaction of metal atoms with CH_3X, the methylmetal halide complex (CH_3-MX) is formed first and the following α-hydrogen migration leads to the methylidene complex. The dramatic increase of $CH_2=TaHX$ indicates that conversion to the methylidene complex from CH_3-TaX is spontaneous and requires essentially no activation energy This is in line with the previous and present results that the single-bonded insertion complexes of the third-row transition metals are not trapped and identified in the IR spectra.[4,9,12,13,15] Note from Figures 9 and 11 that the third-row $CH_2=MHF$ complex is the most stable, whereas the first-row CH_3-MF is the most stable.

However, a similar increase of the methylidene complex in annealing has not been observed in reactions of Ta with CH_3F and CH_4 and in reactions of other third-row transition metals

TABLE 11: Geometrical Parameters and Physical Constants Calculated for the $CH{\equiv}NbH_2X^-$ and $CH{\equiv}TaH_2X^-$ Anion Complexes[a]

parameters	$CH{\equiv}NbH_2F^-$	$CH{\equiv}NbH_2Cl^-$	$CH{\equiv}NbH_2Br^-$	$CH{\equiv}TaH_2F^-$	$CH{\equiv}TaH_2Cl^-$	$CH{\equiv}TaH_2Br^-$
$r(C-H_1)$	1.091	1.089	1.089	1.088	1.087	1.087
$r(C-M)$	1.808	1.794	1.792	1.829	1.820	1.818
$r(M-H_2)$	1.837	1.825	1.823	1.839	1.829	1.826
$r(M-X)$	1.976	2.437	2.602	1.967	2.428	2.595
$\angle CMX$	112.4	112.9	113.0	113.7	114.5	114.6
$\angle CMH_2$	101.4	99.6	99.4	102.1	100.7	100.4
$\angle H_2MX$	113.6	115.3	115.7	112.5	114.5	115.0
$\angle H_2MH_3$	113.0	111.8	111.3	113.0	110.4	109.6
$\angle H_1CM$	169.0	173.7	175.0	168.1	173.3	174.8
$\Phi(H_1CMH_2)$	121.7	122.9	123.2	121.5	123.3	123.8
$\Phi(H_1CMX)$	0.0	0.0	0.0	0.0	0.0	0.0
mol. sym.	C_s	C_s	C_s	C_s	C_s	C_s
$q(C)^b$	−1.14	−0.95	−0.97	−0.83	−0.75	−0.72
$q(H_1)^b$	−0.01	0.03	0.02	0.07	0.09	0.09
$q(H_2)^b$	−0.39	−0.53	−0.52	−0.44	−0.42	−0.41
$q(H_3)^b$	−0.39	−0.53	−0.52	−0.44	−0.42	−0.41
$q(M)^b$	1.51	1.88	1.77	1.23	1.42	1.22
$q(X)^b$	−0.57	−0.91	−0.78	−0.59	−0.93	−0.78
μ^c	2.07	1.91	3.43	2.88	2.28	3.12
state[d]	$^1A'$	$^1A'$	$^1A'$	$^1A'$	$^1A'$	$^1A'$
ΔE^e	131.8 (112.0)	130.4 (110.6)	130.9 (110.0)	143.2 (133.2)	140.1 (130.2)	139.9 (130.0)

[a] Bond lengths and angles are in angstroms and degrees. Calculated using B3LYP/6-311++G(3df, 3pd)/SDD. [b] Mulliken atomic charge. [c] Molecular dipole moment in D. [d] Electronic state. [e] Binding energies in kcal/mol relative to $M + CH_3X$ (relative to $M^- + CH_3X$).

with CH_3Cl and CH_3Br. This suggests that the C−X insertion reactions of Ta with CH_3Cl and CH_3Br can also be thermally initiated unlike other systems, which will eventually lead to the formation of $CH_2{=}TaHX$. The electron-rich halides most likely provide an efficient reaction path with the electron deficient third-row transition metal in the matrix. At this point, it is not clear why other third-row transition metals do not show a similar increase of methylidene in annealing. Closer theoretical as well as experimental investigation in the future on this subject would shed light on the extraordinary reactivity of Ta with the halides.

Ligand effects similar to those of Nb counterparts are observed for the methylidene complexes from the reaction of Ta with CH_3Cl and CH_3Br. With increasing halogen size, more electron density is allowed to remain in the carbon−metal double bond, and as a result, the agostic distortion increases (Figure 12) and the carbon−tantalum double bond becomes stronger (the stretching frequency and bond length increases and decreases, respectively). Therefore, it is reasonable to conclude that, for the group 5 metals, the agostic interaction increases with increasing halogen size, similar to group 4 metals.[3,8] The ligand effects of group 6 metal complexes will be examined and reported soon.

Like in other third-row metal systems, no absorption from the single-bonded insertion complex (CH_3-TaX (X = F, Cl, and Br)) is observed. Parallel to the case of $Nb + CH_3X$, only a weak hydrogen stretching absorption arises from $CH{\equiv}TaH_2Cl^-$ as shown in Figure 7, and no absorption from $CH{\equiv}TaH_2Br^-$ is observed, indicating that the anionic methylidyne complex is less favored with increasing halogen size, probably because CH_3Cl and CH_3Br themselves behave as electron capturing agents as described above.

Conclusions

Reactions of laser-ablated group 5 metal atoms with methyl halides in excess argon have been carried out during condensation at 8 K. In the reaction of V with CH_3F, the C−F insertion complex is the primary product, which converts to the methylidene complex ($CH_2{=}VHF$) via α-hydrogen migration on UV photolysis afterward. The methyl and methylidene complexes form a persistent photoreversible pair and show a kinetic isotope effect for the yield of $CD_2{=}VDF$. The reaction of Ta with CH_3F provides $CH_2{=}TaHF$ and $CH{\equiv}TaH_2F^-$, but the C−F insertion complex (CH_3-TaF) is not identified. Absence of the C−F insertion complex is probably due to its relatively higher energy. Along with recent preparation of anionic methylidyne complexes ($CH{\equiv}MH_3^-$ and $CH{\equiv}MH_2F^-$) in reactions of Nb and Ta,[14,15] the present results suggest that formation of the anionic species is a general property of the group 5 transition metals.

Reactions of the heavy group 5 metals (Nb and Ta) with methyl halides (CH_3Cl and CH_3Br) have also been carried out. Strong absorptions of the methylidene complexes are observed while the absorptions of the anionic methylidyne are mostly too weak to be observed. Clearly, the anionic methylidyne complexes become less favored with increasing halogen size, probably because the heavy halides themselves behave as electron capturing agents. The methylidene complexes are more agostically distorted with increasing halogen size, similar to the group 4 metal systems. Interestingly enough, the tantalum methylidenes of the heavy halides increase dramatically in the process of annealing, suggesting that both formation of the C−X insertion complex and conversion to the methylidene complex are spontaneous and require essentially no activation energy.

Acknowledgment. We gratefully acknowledge financial support from NSF Grant CHE 03-52487 to L.A.

References and Notes

(1) Cho, H.-G.; Andrews, L. *J. Phys. Chem. A* **2004**, *108*, 6294 (Ti + CH_3F).

(2) Andrews, L.; Cho, H.-G.; Wang, X. *Inorg. Chem.* **2005**, *44*, 4834 (Ti + CH_4).

(3) Cho, H.-G.; Andrews, L. *Inorg. Chem.* **2005**, *44*, 979 (Ti + CH_3X).

(4) Cho, H.-G.; Wang, X.; Andrews, L. *Organometallics* **2005**, *24*, 2854 (Hf + CH_4).

(5) Cho, H.-G.; Andrews, L. *J. Am. Chem. Soc.* **2004**, *126*, 10485 (Zr + CH_3F).

(6) Andrews, L.; Cho, H.-G.; Wang, X. *Angew. Chem., Int. Ed.* **2005**, *44*, 113 (Zr + CH_4).

(7) Cho, H.-G.; Wang, X.; Andrews, L. *J. Am. Chem. Soc.* **2005**, *127*, 465 (Zr + CH_4).

(8) Cho, H.-G.; Andrews, L. *Chem. Asian J.* **2006**, *1*, in press (Zr, Hf + CH_3X).

(9) Cho, H.-G.; Andrews, L. *Organometallics* **2004**, *23*, 4357 (Hf + CH_3F).

(10) Cho, H.-G.; Andrews, L. *J Am. Chem. Soc*. **2005**, *127*, 8226 (Mo + CH_4).

(11) Cho, H.-G.; Andrews, L. *Chem.−Eur. J*. **2005**, *11*, 5017 (Mo + CH_3F).

(12) Cho, H.-G.; Andrews, L.; Marsden, C. *Inorg. Chem.* **2005**, *44*, 7634 (W + CH_4).

(13) Cho, H. G.; Andrews, L. *Organometallics* **2005**, *24*, 5678 (Cr, W + CH_3F).

(14) Cho, H. G.; Andrews, L. *Organometallics* **2005**, *25*, 477 (Nb + CH_3F).

(15) Cho, H. G.; Andrews, L. *J. Phys. Chem.* **2006**, *110*, 3886 (V, Nb, and Ta + CH_4).

(16) Andrews, L.; Cho, H.-G. *Organometallics*, **2006**, *25*, in press (review article).

(17) (a) Schrock, R. R. *Chem. Rev*. **2002**, *102*, 145. (b) Buchmeiser, M. R. *Chem. Rev*. **2000**, *100*, 1565.

(18) Scherer, W.; McGrady, G. S. *Angew. Chem., Int. Ed.* **2004**, *43*, 1782.

(19) Klabunde, K. J.; Tanaka. Y. *J. Am. Chem. Soc*. **1983**, *105*, 3544.

(20) Klotzbucher, W. E.; Mitchell, S. A.; Ozin, G. A. *Inorg. Chem.* **1977**, *16*, 3063.

(21) (a) Billups, W. E.; Konarski, M. M.; Hauge, R. H.; Margrave, J. L. *J. Am. Chem. Soc*. **1980**, *102*, 7393. (b) Ozin, G. A.; McIntosh, D. F.; Mitchell, S. A.; Garcia-Prieto, J. *J. Am. Chem. Soc*. **1981**, *103*, 1574.

(22) Wang, G.; Chen, M.; Zhou, M. *Chem. Phys. Lett.* **2005**, *412*, 46.

(23) (a) Zhou, M. F.; Andrews, L. *J. Phys. Chem. A* **1998**, *102*, 8251. (b) Wang, X.; Andrews, L. *J. Phys. Chem. A* **2003**, *107*, 570.

(24) Andrews, L.; Citra, A. *Chem. Rev*. **2002**, *102*, 885 and references therein.

(25) Kudin, K. N.; Burant, J. C.; Millam, J. M.; Iyengar, S. S.; Tomasi, J.; Barone, V.; Mennucci, B.; Cossi, M.; Scalmani, G.; Rega, N.; Petersson, G. A.; Nakatsuji, H.; Hada, M.; Ehara, M.; Toyota, K.; Fukuda, R.; Hasegawa, J.; Ishida, M.; Nakajima, T.; Honda, Y.; Kitao, O.; Nakai, H.; Klene, M.; Li, X.; Knox, J. E.; Hratchian, H. P.; Cross, J. B.; Adamo, C.; Jaramillo, J.; Gomperts, R.; Stratmann, R. E.; Yazyev, O.; Austin, A. J.; Cammi, R.; Pomelli, C.; Ochterski, J. W.; Ayala, P. Y.; Morokuma, K.; Voth, G. A.; Salvador, P.; Dannenberg, J. J.; Zakrzewski, V. G.; Dapprich, S.; Daniels, A. D.; Strain, M. C.; Farkas, O.; Malick, D. K.; Rabuck, A. D.; Raghavachari, K.; Foresman, J. B.; Ortiz, J. V.; Cui, Q.; Baboul, A. G.; Clifford, S.; Cioslowski, J.; Stefanov, B. B.; Liu, G.; Liashenko, A.; Piskorz, P.; Komaromi, I.; Martin, R. L.; Fox, D. J.; Keith, T.; Al-Laham, M. A.; Peng, C. Y.; Nanayakkara, A.; Challacombe, M.; Gill, P. M. W.; Johnson, B.; Chen, W.; Wong, M. W.; Gonzalez, C.; Pople, J. A. *Gaussian 03*, revision B.04; Gaussian, Inc.: Pittsburgh, PA, 2003.

(26) (a) Becke, A. D. *J. Chem. Phys.* **1993**, *98*, 5648. (b) Lee, C.; Yang, Y.; Parr, R. G. *Phys. Rev. B* **1988**, *37*, 785.

(27) Frisch, M. J.; Pople, J. A.; Binkley, J. S. *J. Chem. Phys.* **1984**, *80*, 3265.

(28) Andrae, D.; Haeussermann, U.; Dolg, M.; Stoll, H.; Preuss, H. *Theor. Chim. Acta* **1990**, *77*, 123.

(29) (a) Xiao, Z. L.; Hauge, R. H.; Margrave, J. L. *J. Phys. Chem*. **1991**, *95*, 2696. (b) Van Zee, R. J.; Li, S.; Weltner, W., Jr. *J. Chem. Phys.* **1995**, *102*, 4367 (V + H_2).

(30) Wang, X.; Andrews, L. Unpublished data (Nb, Ta + H_2).

(31) (a) Pyykko, P.; Desclaux, J. P. *Chem. Phys. Lett*. **1977**, *50*, 503. (b) Pyykko, P.; Snijders, J. G.; Baerends, E. J. *Chem. Phys. Lett.* **1981**, *83*, 432. (c) Ziegler, T.; Snijders, J. G.; Baerends, E. J. *J. Chem. Phys*. **1981**, *74*, 1271. (d) Pyykko, P. *Chem. Rev*. **1988**, *88*, 563.